Marine Geophysical Researches **23:** 443–469, 2002.

Geology of the Atlantis Massif (Mid-Atlantic Ridge, 30° N): Implications for the evolution of an ultramafic oceanic core complex

Donna K. Blackman[1], Jeffrey A. Karson[2], Deborah S. Kelley[3], Johnson R. Cann[4], Gretchen L. Früh-Green[5], Jeffrey S. Gee[1], Stephen D. Hurst[7], Barbara E. John[6], Jennifer Morgan[4], Scott L. Nooner[1], D. Kent Ross[8], Timothy J. Schroeder[6] & Elizabeth A. Williams[2]

[1]*Scripps Institution of Oceanography, La Jolla, CA 92093-0225 USA;* [2]*Division of Earth & Ocean Sciences, Duke University, Durham, NC 27708-0230 USA;* [3]*School of Oceanography, University of Washington, Seattle, WA 98195-7940 USA;* [4]*Department of Earth Sciences, University of Leeds, Leeds LS2 9JT UK;* [5]*Institut fur Mineralogie & Petrographie, ETH-Zentrum, CH-8092 Zurich, Switzerland;* [6]*Department of Geology and Geophysics, University of Wyoming, Laramie, WY 80271 USA;* [7]*Department of Geology, University of Illinois, Urbana, IL 61801 USA;* [8]*Department of Geology & Geophysics, University of Hawaii, Honolulu, HI 96822 USA*

Received 18 March 2003, accepted 29 October 2003

Abstract

The oceanic core complex comprising Atlantis Massif was formed within the past 1.5–2 Myr at the intersection of the Mid-Atlantic Ridge, 30° N, and the Atlantis Transform Fault. The corrugated, striated central dome prominently displays morphologic and geophysical characteristics representative of an ultramafic core complex exposed via long-lived detachment faulting. Sparse volcanic features on the massif's central dome indicate that minor volcanics have penetrated the inferred footwall, which geophysical data indicates is composed predominantly of variably serpentinized peridotite. In contrast, the hanging wall to the east of the central dome is comprised of volcanic rock. The southern part of the massif has experienced the greatest uplift, shoaling to less than 700 m below sea level, and the coarsely striated surface there extends eastward to the top of the median valley wall. Steep landslide embayments along the south face of the massif expose cross sections through the core complex. Almost all of the submersible and dredge samples from this area are deformed, altered peridotite and lesser gabbro. Intense serpentinization within the south wall has likely contributed to the uplift of the southern ridge and promoted the development of the Lost City Hydrothermal Field near the summit. Differences in the distribution with depth of brittle deformation observed in microstructural analyses of outcrop samples suggest that low-temperature strain, such as would be associated with a major detachment fault, is concentrated within several tens of meters of the domal surface. However, submersible and camera imagery show that deformation is widespread along the southern face of the massif, indicating that a series of faults, rather than a single detachment, accommodated the uplift and evolution of this oceanic core complex.

Introduction

The fundamental component of oceanic core complexes (OCC) is an uplifted, dome-like exposure of variably deformed lower crustal and upper mantle rocks that has been unroofed by extreme tectonic extension along a spreading center (Cann et al., 1997; Dick et al., 1991; 2000; Karson, 1990; Tucholke and Lin, 1994; Tucholke et al., 1998). Footwall or lower plate rocks of OCC are separated from structurally higher, faulted upper crust by moderately to gently dipping normal or detachment faults. The upper crustal blocks may be multi-kilometer in lateral extent and tilted back along the detachment, or smaller klippe may be all that remains in contact with the exposed footwall. In some cases basaltic lavas, clastic sedimentary rocks, pelagic deposits, or some combination of these, overlie the basement.

A system of detachment faulting appears to operate at inside corners in some areas for several million years, resulting in the development of a series of topographic highs that are spread off axis (Karson, 1998; Tucholke et al., 1998). We refer to the series of tectonic features thus generated as OCC, the implication being that this style of rifting is maintained throughout the development of the whole group of faults,

footwall blocks, and hanging wall blocks. Some of the topographic highs expose large corrugated detachment surfaces that contain 'megamullions' comprised of domal highs and associated swales, which extend in the slip-parallel direction (Tucholke et al., 1998)). Where the extent of subsurface exposure is not as great, the massifs may contain mid-upper crustal rocks uplifted to the seafloor (Karson, 1990, 1998).

Swath bathymetry data were key to initial recognition of most identified OCC, but the distinctive seafloor morphology alone leaves unanswered many questions about the structure and possible origin of these domal massifs. At present, there is no single tectonic template for the evolution of these distinctive features, which are a persistent feature of slow-spreading ridges, produced episodically amongst the more typical abyssal hills. Similar to continental core complexes, there is substantial diversity in terms of the rock types involved, the structures, and the settings of OCC. The core of some complexes appears to be dominantly serpentinite with lesser amounts of gabbro (Blackman et al., 1998; 'Description of Subareas' section, below; Escartín and Cannat, 1999). Others have significant gabbroic sections with related metamorphic rocks (Dick et al., 1991, 2000; Gillis et al., 1993; Karson, 1990, 1999; Kelley et al., 1993; Karson and Lawrence, 1997). In some cases, dramatic unroofing (>2 km) has been documented (Kelley and Delaney, 1987; John et al., 2002) whereas in others the amount of unroofing is unclear and significant uplift may not be necessary to account for the geologic features present. Initial hypotheses suggested that OCC form during intervals of spreading with low magma supply (Karson, 1990; Mutter and Karson, 1992; Tucholke and Lin, 1994), yet the large volume of gabbroic rock sampled at Atlantis Bank, from ODP Site 735B (Dick et al., 2000), seems to be inconsistent with this view (Karson, 1998).

Bathymetric corrugations, finer scale striations, and outcrop-scale slickenlines that are observed on domal surfaces of OCC are interpreted to result from slip on major normal faults (Cann et al., 1997; Escartín and Cannat, 1999; Karson, 1990; Reston et al., 2002; Searle et al., 1998; Tucholke et al., 1998). Direct observations and sampling of the corrugated surfaces support the interpretation that they are exposed brittle faults (Karson and Dick, 1983; MacLeod et al., 2002; Tucholke et al., 2001). The original dip of these fault surfaces is unknown, but must be related to the nature of deformation of the footwall of the complex. The 'rolling hinge' model of core complex formation predicts that large block rotations would characterize OCC formation (Wernicke and Axen, 1988; Buck, 1988; Lavier et al., 1999).

In this paper we report recent observations of morphology and geology at the Atlantis Massif. The origin of the massif is addressed using integrated analyses of multiple data sets, including high-resolution side-scan sonar imagery, direct seafloor observations, sampling of outcrop geology, gravity, seismic, and magnetic anomaly results. In concert these data provide constraints on the subsurface structure of the massif that, in turn, allows us to address the structural evolution of this OCC.

Setting of the Atlantis Massif oceanic core complex

The Atlantis Massif is located at the inside corner of the eastern ridge-transform intersection (RTI) of the MAR and Atlantis Transform Fault (ATF) at about 30° N (Figure 1). The ATF is a right-stepping (sinistral-slipping) transform fault that offsets the MAR axis by ~75 km. The Atlantis Massif is typical of other dome-like seafloor massifs in this part of the central North Atlantic, including several in the immediate vicinity of the ATF (Blackman et al., 1998; Cann et al., 1997).

Morphotectonic Framework

On a broad scale, Atlantis Massif is part of a 25-km-long, morphologically continuous ridge that defines the western side of the median valley of the MAR. This ridge is bounded on the west by a series of steep, west-facing scarps located 15–20 km west of the median valley. In the south, the massif is truncated by a steep, deeply-embayed escarpment that marks the edge of the ATF valley. In the north, the smoothly arched, corrugated dome of the massif merges with a lineated series of abyssal hills, which are defined by relatively closely spaced, asymmetrical, axis-parallel ridges and valleys. These are interpreted as tilted fault blocks of basaltic material (Blackman et al., 1998).

The smoothly arched upper surface of the 'Central Dome' of the massif, at ~1800 m water depth, slopes down to the east (~11°) toward the median valley and gently to the west on the western side of the massif (Figure 2). The bathymetric "corrugations" on the dome surface have wavelengths of ~1000 m, amplitudes of tens of meters, and lengths of several kilometers (Cann et al., 1997). These are parallel to

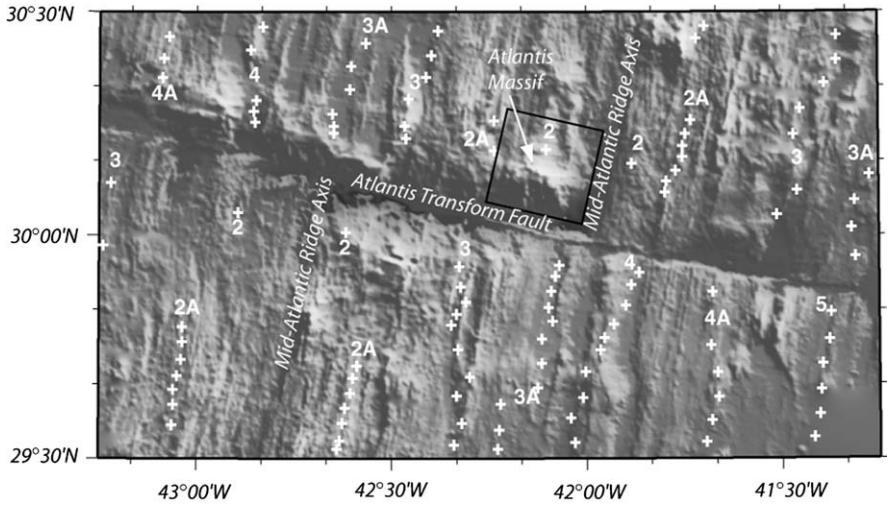

Figure 1. Grayshade bathymetry and magnetic anomaly picks on the Mid-Atlantic Ridge near Atlantis Transform Fault. Dark shade indicates deep seafloor and light indicates shallow; illumination is from the NE. Crosses show anomaly picks from Pariso et al. (1996) except for anomaly 2 pick which is from Zervas et al. (1995). Location of Atlantis Massif is shown and box corresponds to region in Figure 2a.

finer scale lineations, up to 3 km long in *TOBI* side-scan sonar data, which are referred to as "striations" (Cann et al., 1997). The Central Dome is sharply bounded in the east by a ∼20 km-long ridge that defines the top of the western median valley wall of the MAR (Figure 2). The eastern flank of this ridge is relatively steep and linear compared to the more gently sloping and irregular west side. *TOBI* side-scan sonar images on the gently sloping side show conical hills and hummocky terrain interpreted as constructional basaltic features. This 'Eastern Block' is interpreted as a fault-bounded block (i.e. allochthonous, hanging wall) that lies structurally above the corrugated detachment fault surface of the Central Dome (Cann et al., 1997).

The southern third of the massif is dominated by an asymmetric, transform-parallel ridge, the 'Southern Ridge' (Figure 2) that rises from the Central Dome to depths of less than 700 m. The Southern Ridge is bounded in the south by the steep 'South Wall', which defines the edge of the ATF valley. This escarpment provides a window into the internal structure of the core of the massif. The southeastern shoulder of the Southern Ridge slopes gently toward the MAR median valley, but it is truncated by a steep scarp that faces the RTI. Westward the Southern Ridge slopes away from the spreading axis. The summit peak is located about midway along the length of the Southern Ridge. The Lost City hydrothermal vent field occurs just below the top of the South Wall near the summit. This field of active and inactive, hydrothermal structures is believed to be driven by ongoing subsurface serpentinization reactions (Kelley et al., 2001; Früh-Green et al., 2003).

Geophysical framework

The domal top of the Atlantis Massif is about 15 km west of the morphologic axis of the MAR (Figure 2). At this latitude the MAR is spreading at an average half-rate of 12 mm/yr (Zervas et al., 1995). Based on this spreading rate and its distance from the spreading axis, the massif consists of lithosphere spanning 0.5 to 2.0 Myr in age. Pariso et al. (1996) and Zervas et al. (1995) determine that the western edge of Atlantis Massif lies near anomaly 2 (Figure 1). This pick corresponds to a recent local spreading rate that is ∼25% slower on the west flank than the regional average.

Mantle Bouguer gravity anomaly highs are skewed toward the eastern and southern slopes of the Atlantis Massif, indicating that lower crustal and upper mantle rocks are not symmetrically distributed at depth beneath the topographic high (Blackman et al., 1998). Cross-axis gravity profiles are well matched by models that have a central core with densities 200–400 kg/m^3 greater than the surrounding crust and bounded by moderately east- and west-dipping interfaces (Blackman et al., 1998; Nooner et al., 2003). The east-dipping interface in these models of the central portion of Atlantis Massif may correspond to the base of a serpentinized detachment zone that extends below the

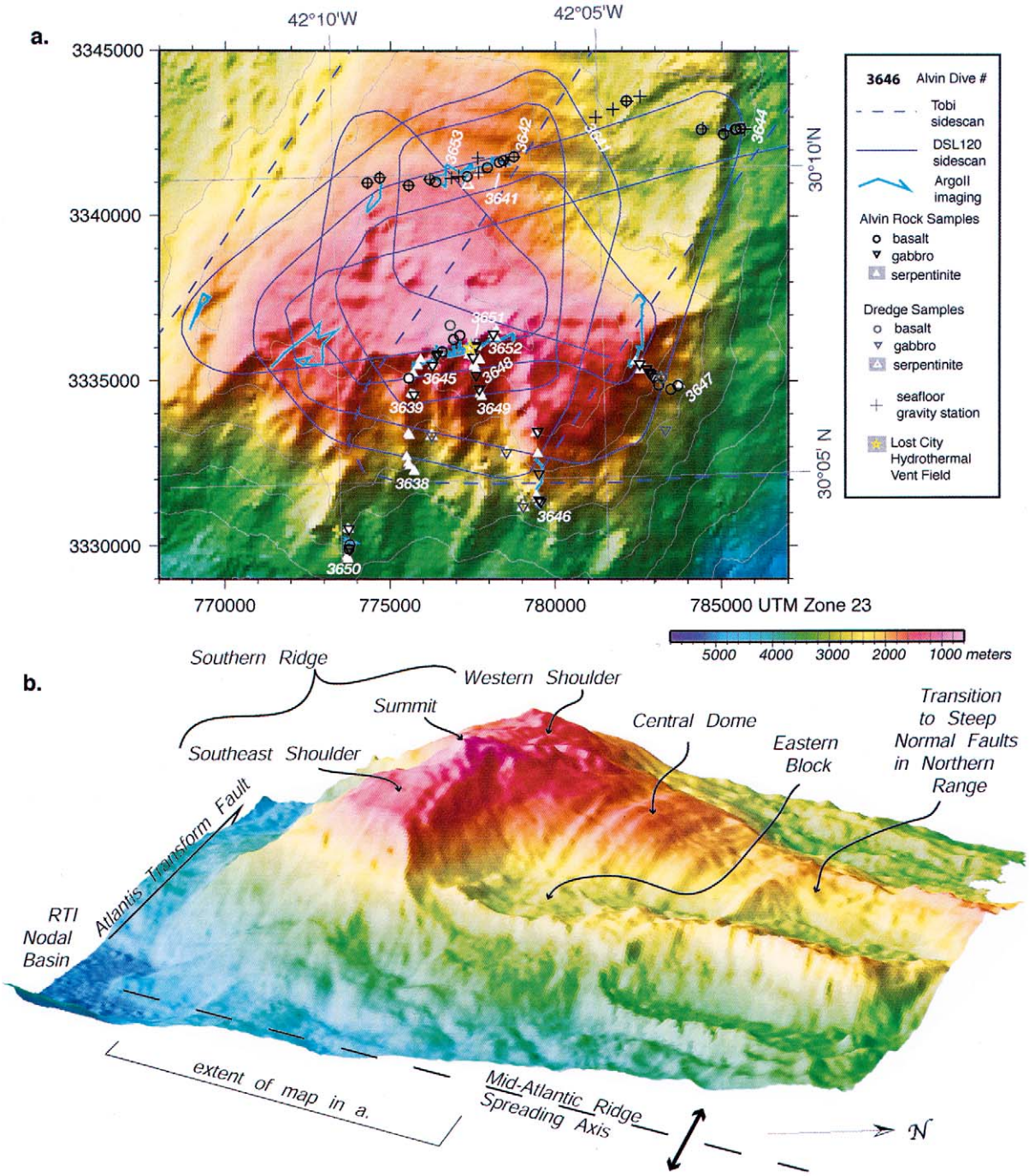

Figure 2. Atlantis Massif at the eastern MAR-ATF intersection. (a) Location of *DSL-120* and *TOBI* side-scan sonar tracks, *Argo II* imaging surveys, *Alvin* dives (numbers are positioned at start of each transect), and rock samples. Left and lower axes are annotated in UTM coordinates (labels in meters). Basic rock types are shown. Bathymetric base map is from 1996 cruise *CD100*, 100 m grid interval, contours at 500 m intervals starting at 1000 m. Illumination is from NW. (b) Large-scale morphology of the Atlantis Massif from WSW-looking perspective shows major morphotectonic features. Vertical exaggeration is ~1.8, illumination is from SE and color scale is the same as in (a).

seafloor from the corrugated domal surface toward the median valley. North of the corrugated dome where the topographic high extends another ~10 km, average crustal density (2850 kg/m^3, Blackman et al., 1998) is more typical of that expected for normal Atlantic crust.

Seismic refraction data at the central dome of Atlantis Massif indicate that mantle velocities (~8.0 kms^{-1}) occur within several hundred meters of the surface (Detrick and Collins, 1998). The distribution of the high velocity material is not tightly constrained by these data but the lateral extent must be at least of the order of a few kms. The seismic velocity gradient in the central Atlantis Massif is similar to that of other MAR sites where serpentinized peridotite has been drilled or mapped on the seafloor (Collins et al., 2001). Seismic velocities beneath the southern ridge of the massif are also high (~7.5 kms^{-1}), within a range that could reflect either partly serpentinized peridotite and/or gabbro (Detrick and Collins, 1998).

MARVEL2000 data acquisition

The goal of our recent investigation of the Atlantis Massif (*MARVEL* = Mid-Atlantic Ridge Vents and Extended Lithosphere) was to better define the morphology and geology of key parts of the massif to test, and refine hypotheses regarding its origin as an OCC. The 39-day cruise aboard the *R/V Atlantis* (*AT3-60*) took place November-December, 2000. Our investigations were concentrated in two main areas: (1) a spreading-parallel corridor from the top of the western median valley wall across the Eastern Block and the Central Dome, and (2) the southern face of the massif where cross-sectional exposures of the footwall of the core complex were expected. Transponder networks were deployed in each of these areas to provide navigation for all near-bottom investigations. In both areas we collected high-resolution side-scan sonar data, seafloor video and digital still imagery, submersible observations, and rock samples.

The *DSL-120* side-scan sonar sled was towed ~100 m above the seafloor to obtain backscatter and phase bathymetry data in the 120 kHz band (Figure 2a). During a 3.5-day survey, we mapped major regions of the southern half of the massif and its flanks. Portions of the South Wall, Southern Ridge, and the Central Dome were imaged almost 100%; the east and west flanks were only partially covered (Figure 3). Backscatter artifacts include symmetrical patterns arising from receiver cross-talk in areas of especially strong acoustic backscatter and, as expected, a lack of returns on the downslope side of tracks traversing across steep terrain.

Alvin submersible dives (15) and *Argo II* imaging surveys (13) were targeted on likely outcrop areas identified on the basis of backscatter pattern and intensity and bathymetric characteristics (Figure 2). Nine *Alvin* dives and 8 *Argo II* surveys were located along the South Wall and Southern Ridge at depths from 3100 m to 700 m. Three *Argo II* surveys, four full *Alvin* dives, and a short engineering dive were completed within the spreading-parallel corridor for collection of seafloor gravity measurements (Nooner et al., 2003), rock sampling, and observations.

Video and digital still cameras (DSC) on the *Argo II* sled were configured in a vertically down-looking mode for all of the surveys on the summit of the massif and in a 30° downward-looking orientation for steep scarps. Two different types of surveys were conducted. In some areas, long transects were made to collect reconnaissance ground-truth data over areas with distinctive backscatter characteristics. In other places, with extensive basement outcrop , closely spaced (5–10 m), subparallel transects were conducted in areas as large as 100 m square. Overlapping DSC images from these surveys were merged to create mosaics of outcrop areas several meters to a few tens of meters in scale.

Alvin dives provided direct observations and samples of the Central Dome, fault scarps on the edge of the Eastern Block, and the South Wall. Dives covered 1–2 km distance and provided continuous video and 35 mm camera coverage of the seafloor. Samples were collected at regular intervals and also from features of particular interest.

Two dredges on the flanks of the southeast shoulder of the Southern Ridge recovered a variety of partially serpentinized peridotites and variably deformed and metamorphosed gabbroic rocks.

Post-cruise analyses of data included merging of *DSL-120* side-scan sonar data with the *TOBI* data from a previous cruise (RRS Charles Darwin – *CD100*) (Blackman et al., 1998; Cann et al., 1997). The 30 kHz *TOBI* side-scan system was towed about 500 m above the seafloor, therefore, the image resolution is several meters, in contrast to ~2 m for *DSL-120*. *Alvin* and *Argo II* data were integrated to document the nature of the outcrop in key survey areas. In addition, DSC images from many *Argo II* survey areas were mosaicked to create large-scale views of the seafloor outcrop (few hundred meters square). Initial petrological data were

summarized (online supplement Table 1 lists brief descriptions of all MARVEL samples).

Descriptions of the Subareas of Atlantis Massif

The bathymetric and side-scan sonar data provide a morphotectonic framework for the geology of key subareas of the Atlantis Massif. The side-scan mosaic in Figure 3 shows all of the *DSL-120* tracks and a portion of the *TOBI* tracks. Where tracks cross, one track (or a portion thereof) is chosen to overlie the other; in this figure the choices were made to illustrate overall structure. In subsequent figures that show side-scan data, the choice of overlying track may differ if the insonification angle of the other track increases the visibility of features being discussed. In the following descriptions, we use x,y coordinates in UTM zone 23 to locate specific features of interest.

Spreading-parallel corridor

This component of the *MARVEL* study focused on a swath of seafloor extending from the top of the western median valley wall of the MAR, about 15 km north of the ATF, to the WSW, roughly parallel to the relative plate motion direction. From east to west this corridor includes the Eastern Block of basaltic material, the corrugated Central Dome, and a less-well mapped region in the western part of the massif.

Eastern block. The MARVEL data are consistent the earlier interpretation (Cann et al., 1997; Blackman et al., 1997) of the Eastern Block as an allochthonous block of basaltic material above the detachment fault. Acoustic and morphologic features on top of the Eastern Block include several widely spaced, flat-topped cones and many small mounds that resemble volcanic constructions of the MAR axial valley observed elsewhere (Smith and Cann, 1992) (Figures 3 and 4). The mounds form clusters several hundred meters across and are more abundant on the northern part of the block ($\geq 30° 12' N$).

The southern part of the Eastern Block is a smooth, acoustically absorbing terrain (Figures 3 and 4) interpreted as basalt covered by variably consolidated sediment. The sediment is a few tens of centimeters to 2 m thick. Ripple marks and winnowing of sediment in the area reflect limited current action. This smooth sediment masks the contact between the Eastern Block and the adjacent Central Dome. The east scarp of the Eastern Block consists of a series of near vertical cliffs and intervening, more gently inclined steps (Dive 3644); these components combine to produce an overall slope of about 45°. The cliff at the top edge of the block is ~100 m high and exposes variably fractured pillow basalts (Figure 5) capped by 0.5–2 m of laminated chalk and unconsolidated pelagic ooze. Talus ranging in size from large angular boulders to cobbles buries the base of the scarp. All rocks sampled by *Alvin* or dredged from the eastern scarp and from the top of the Eastern Block are basaltic in composition.

A narrow, NS-trending, east-dipping scarp extends along the break in slope between the dome and the Eastern Block (just west of $x = 782000$, between $y \sim 3340500$ and $y \sim 3341500$). The south end of this long scarp trends southeast, towards a field of mounds interpreted to be volcanic features. The northern end of the scarp strikes northeast, toward the splayed scarps of a northeast-trending ridge that is 50 to 100 m high ($x = 782000$, $y = 3343000$, Figure 3). Pillow basalts were exposed in scarps several meters high that bound a small graben in the latter region of the Eastern Block (Dive 3643, Figure 2a).

Central dome. Linear topographic corrugations are essentially continuous across the full width of the Central Dome (Figure 2). Striae imaged with side-scan sonar do not individually extend the length of the domal surface, however they do occur throughout the corrugated region (Figure 6a). Where they are best developed, the striae can be correlated with exposed linear areas of rubble/breccia (bright reflectors) and intervening sediments (acoustically absorbing so they are dark in the side-scan image), which were observed along an *Argo II* transect. In general, however, individual features in either *Argo II* or *Alvin* imagery were not recognized that might correspond to the striae. This is probably because these features have wavelengths of several tens of meters.

Locally, parallel lineaments trend NE, crossing and truncating the ESE-trending striations ($x = 775500$, $y = 3341000$, Figure 6a). Other areas show complex acoustic backscatter patterns with various orientations, overprinted by the ESE-trending structures ($x = 777000$, $y = 3340500$, Figure 6a). Collectively, these may correspond to complexly oriented layering or metamorphic fabrics exposed on a low-relief surface. Such relationships are not evident in the *TOBI* data, but they are clearly present in the higher resolution *DSL-120* data.

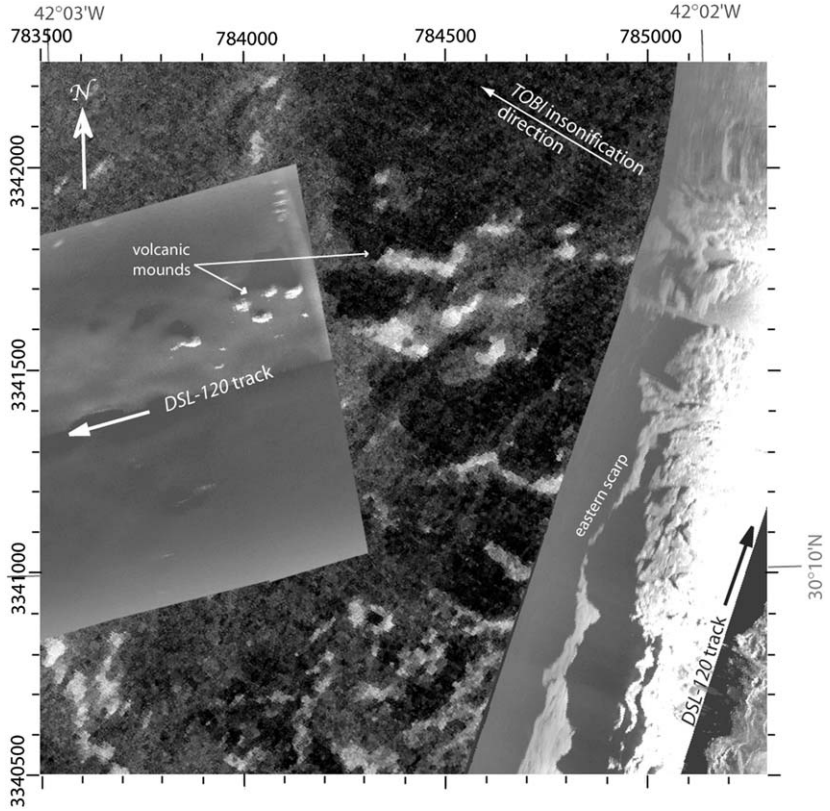

Figure 4. Side-scan sonar data show acoustic features interpreted as volcanic mounds on top of the Eastern Block. Location is shown in Figure 3. A portion of two *DSL-120* swaths are overlain on part of a *TOBI* swath. Cut-away of *DSL-120* track allows comparison of mound signature between the two systems. Steep eastern scarp dips down to the right, it has high reflectivity as do the sides of the small mounds. Low reflectivity sediments surround the mounds, which cast dark acoustic shadows. *Alvin* dive and *Argo II* mosaicking (Figure 5) run were just to the north of the area shown here (Figure 2a).

Large areas with low reflectivity, interpreted as smooth pelagic sediment, are pervasive on the east slope of the Central Dome at seafloor depths greater than ~2000 m. Both large, low reflectivity fields and smaller ponds also occur on the west slope. Variably lithified chalks, commonly a few tens of centimeters thick, drape low-relief topography on the dome. The chalks commonly have dark-stained surfaces and a knobby surface texture reminiscent of elephant skin. Local exposures of rubble, breccia, and (possible) weathered pillows, separated by extensive areas of smooth sediment dotted with sparse blocks of basement material were observed on the western part of the Central Dome (Figure 7a–b).

A 1.5-km^2 patch of sedimented conical hills occurs near the top of the east slope of the Central Dome (x = 779100, y = 3342300). A single, isolated flat-topped cone occurs 2.5 km south of this field (x = 778700, y = 3397000; Figure 3).

Rare patches of exposed bedrock were observed during *Alvin* dives on the Central Dome (Figure 7c). Elsewhere the bedrock was mantled with breccia embedded in lithified carbonate. Overall recovery from the central dome included three samples of fresh basalt (containing fresh olivine), seven of undeformed greenschist-facies metabasalt, one of serpentinite largely replaced by talc, and a sample now composed of talc and chlorite which is probably an altered gabbro. The three samples obtained from bedrock are all of metabasalt.

West Side of the Massif. Coverage of the western side of the Atlantis Massif is very sparse. The break in slope from the smoothly sloping dome top to the west face of the massif is marked by a series of small, few-hundred meter long scarps that are visible on both the bathymetry and side-scan images. A kilometer farther downslope, large, west-facing, en echelon scarps define the main western boundary of the mas-

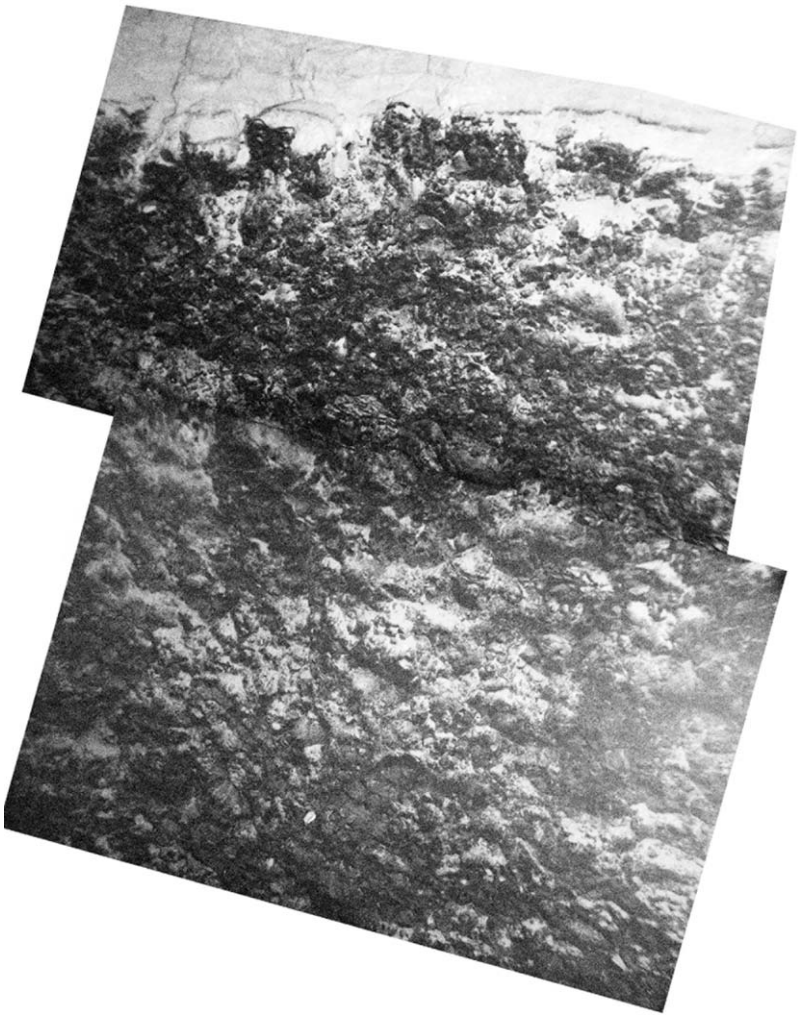

Figure 5. Pillow basalts exposed at the top of the steep fault scarp that bounds the eastern edge of the Eastern Block. Sediment layers blanket the top of the surface, as seen here. Two still camera (*DSC*) images, combined to show a section ∼12 m high, were obtained by *Argo II* at location ∼785200, 3342700 (Figures 2a, 3) at seafloor depth ∼2500 m. Camera view angle is 30° downward.

sif. These extensive scarps are each a few kilometers long and have relief of a few hundred meters (Figure 3 and Blackman et al., 1998, Figure 1 and Plate 4a). *DSL-120* backscatter imagery of some of these large scarps delineate a series of closely spaced, parallel, linear reflectors that are interpreted as stepped, west-facing faults (Figure 3, $x = 773500$, $y = 3343000$). Smaller scarps splay from the large ones (Figure 3, $x = 774000$, $y = 3345000$) and in some places intersect the more extensive faults at high angles ($x = 776000$, $y = 3345000$). Other features are interpreted as sinuous, sediment-filled valleys.

An *Argo II* transect at ∼2000 m depth on the west side of the massif (Figure 2a) encountered mostly sloping, sediment covered talus and some outcrops that appear to be weathered basalt. The outcrops were exposed in a deep notch trending SSW from $x = 769500$, $y = 3337500$, with ∼100–200 m of relief (Figure 3).

Southern Atlantis Massif

The southern part of the Atlantis Massif differs substantially from the spreading-parallel corridor described above. Our investigations of the various areas within this region provide important insights into the development of the Southern Ridge and the evolution of the Atlantis Massif.

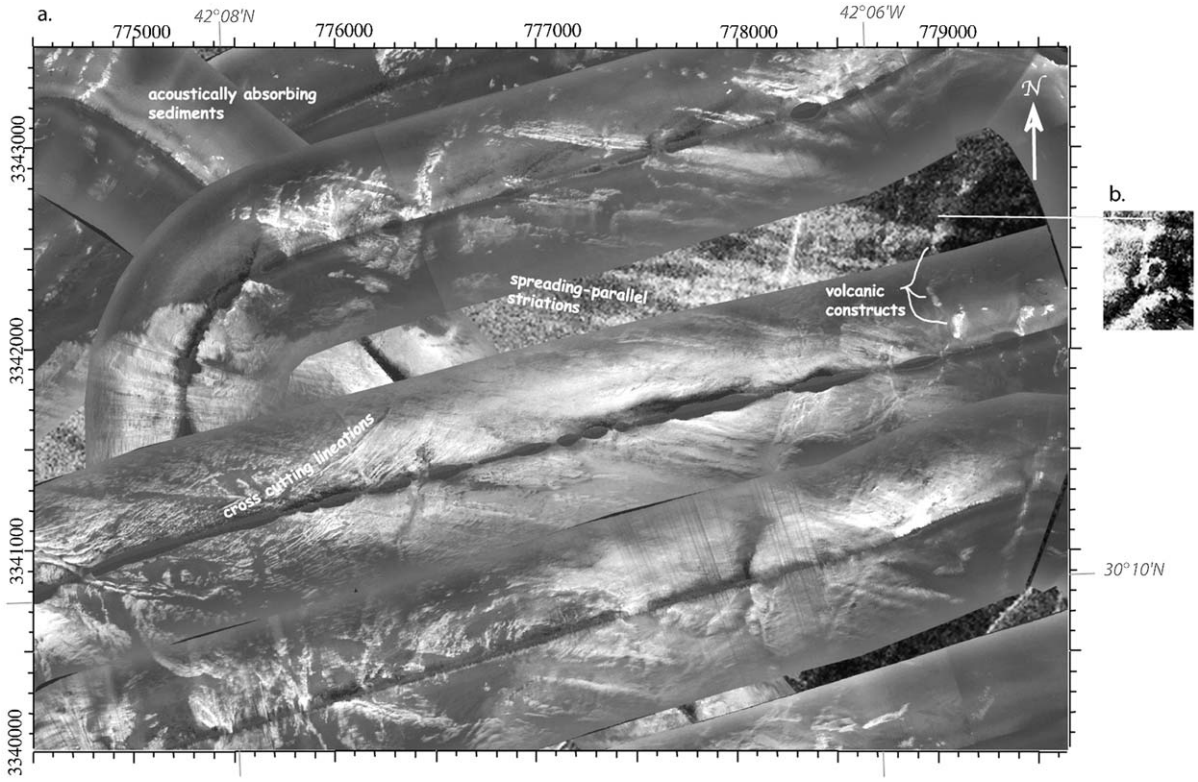

Figure 6. Side-scan sonar data on the Central Dome (location shown in Figure 3). Scales are the same for a and b. (a) *DSL-120* swaths overlay *TOBI* data and show that most striations are parallel to the spreading direction (ESE). A set of smaller linea trending NE have different acoustic character which likely reflects a different origin for this seafloor signature. (b) *TOBI* data show the volcanic constructs labeled on the overlying *DSL-120* swath in (a). Insonification is from NW.

The South Wall. The South Wall of the Atlantis Massif rises from a smooth, gently sloping talus ramp at its base, to a steep, deeply embayed wall (Figures 2a and 3) near its summit. The average slope of the wall is about 40°, but in detail it consists of many near-vertical cliffs with spectacular bedrock exposures, separated by more gently sloping terraces covered by rock debris and pelagic ooze. The steep, arcuate headwall scarps and troughs that trend downslope mark sites of significant mass wasting (Figure 8). These embayments host numerous SW and SE facing cliffs that produce a complex, three-dimensional exposure of variably deformed basement rock. The uppermost few hundred meters of the South Wall is an especially steep interval, with multiple extensive, subvertical (and locally overhanging) cliff exposures.

Side-scan sonar images of the South Wall scarp (Figure 8) show strong reflectors that are indicative of steep cliff faces and shadows typical of very rough terrain. Dense *Argo II* surveys imaged some of the extensive cliff faces (Figure 9 shows a photomosaic from a portion of one survey) and also a few lateral transects across the wall. Several of the *Alvin* dives on the South Wall obtained imagery and samples in *Argo II* survey areas.

Basement material exposed on the South Wall (Figures 9, 10) is dominated by partially to pervasively serpentinized (70–95%) peridotite (Figure 11a–d, online supplement Table 1). Locally, vertical outcrops up to 200 m high are cut by relatively few fractures. Attempts to obtain samples from these sections were unsuccessful so our samples are biased toward more fractured rock types. Some serpentinite outcrops are massive (Figure 10a), however most exposures have a well-developed, narrowly spaced (0.5 m or less) anastomosing foliation (Figures 10b and 11b), typical of many deformed serpentinites (O'Hanley, 1996). Our sampling was not dense enough to allow unique correlation of outcrop-scale foliation to specific microstructures. The outcrop foliation patterns that we observed could be due to either parallel fracturing or to development of ribbon texture. (Figure 11c). The

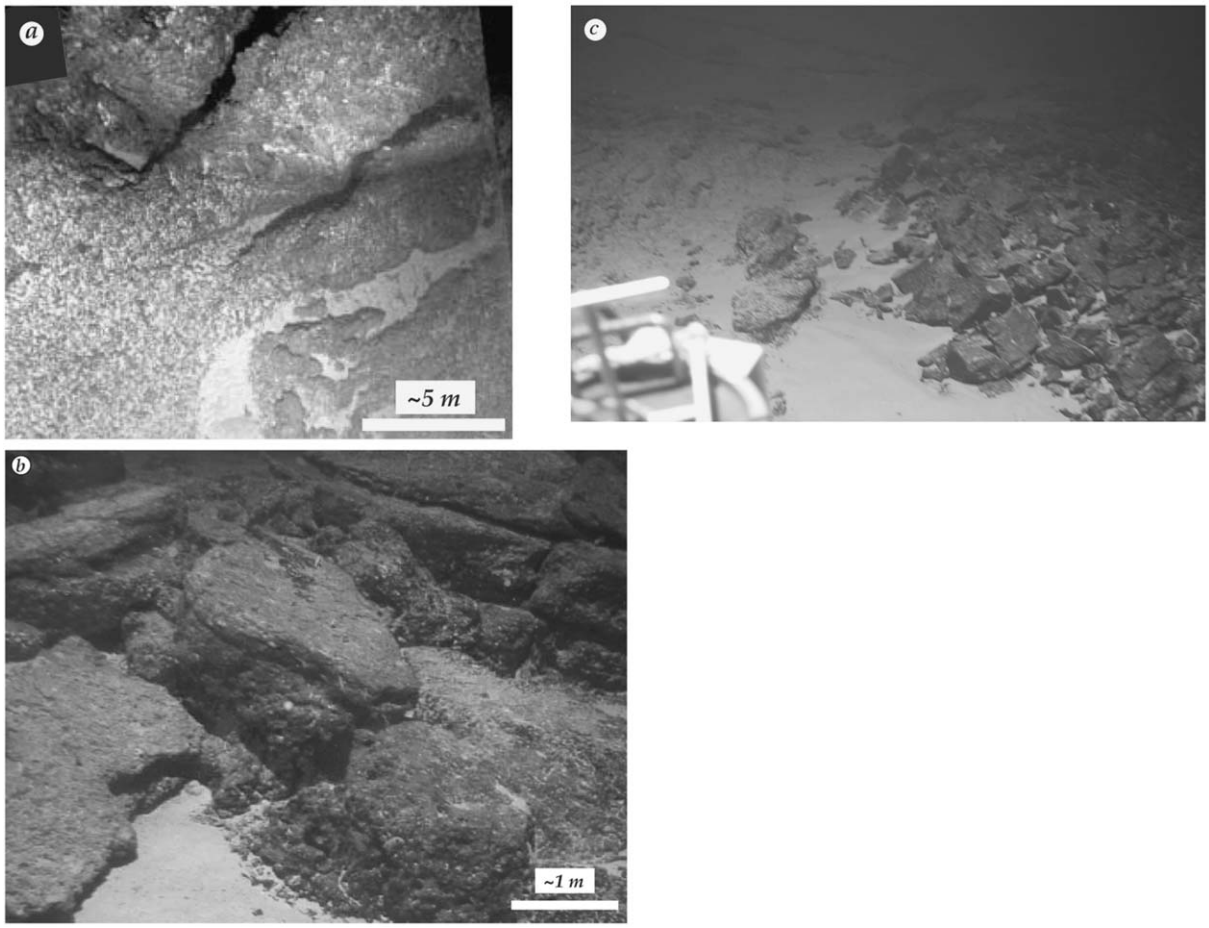

Figure 7. Surface deposits and bedrock on top of the Central Dome. (a) Indurated rubble (metabasalt and serpentinite?) on top of dome is shown by Digital Still Camera mosaic from *Argo II* survey ~774500, 3340500 (Figure 2a, 3) at 1536 m seafloor depth. Camera view is vertical. (b) Sedimentary breccia (indurated rubble) with clasts of metabasalt and serpentinite on top of dome. Photograph by *Alvin* hull-mounted camera at depth 1700 m, westernmost dive (3653) in the spreading-parallel corridor (Figure 2a). (c) *Alvin* photograph shows the edge of an outcrop of basalt that was sampled during Dive 3642. Video taken by *Alvin* shows that this ~20 m × 20 m outcrop includes some fractured pillows.

latter has been documented to parallel both high and low temperature microstructural deformation in similar settings elsewhere on the MAR (e.g. Ceuleneer and Cannat, 1997). The distribution of foliated outcrops is complex and discontinuous throughout the South Wall. However, the orientation of the outcrop foliation appears to be fairly systematic. The apparent dip of the foliation changes from SW in the west, to gently SE in the east across the central-eastern portion of the southern wall. Locally, continuous steeply W- and N-dipping faults cut the foliated serpentinites.

The protolith of the serpentinite is harzburgite. These rocks are commonly cut by veins composed dominantly of talc, tremolite and chlorite (Figure 11e, g), that are interpreted as pathways for metsomatic fluids. In several cases, alteration, veining, and melt-rock reactions are so intense that primary textures of the peridotites are no longer clearly visible (Früh-Green et al., 2001; Schroeder et al., 2001). The suite of samples obtained from the Atlantis Massif resembles ultramafic and gabbroic rocks from other exposures in submarine environments (Cannat et al., 1997; Dick, 1989; Kelley et al., 1993; Gillis et al., 1993; Kelley, 1997; Karson, 1998; Lagabrielle et al., 1998). These rocks record a complex history of deformation and hydrothermal alteration. Multiple generations of veins are present within the various rock types, although static alteration and incomplete serpentinization reactions are common within the peridotites (Früh-Green et al., 2001; Boschi et al., 2002). Metasomatic alteration and formation of talc-bearing mineral assemblages in the peridotites and gabbroic veins is

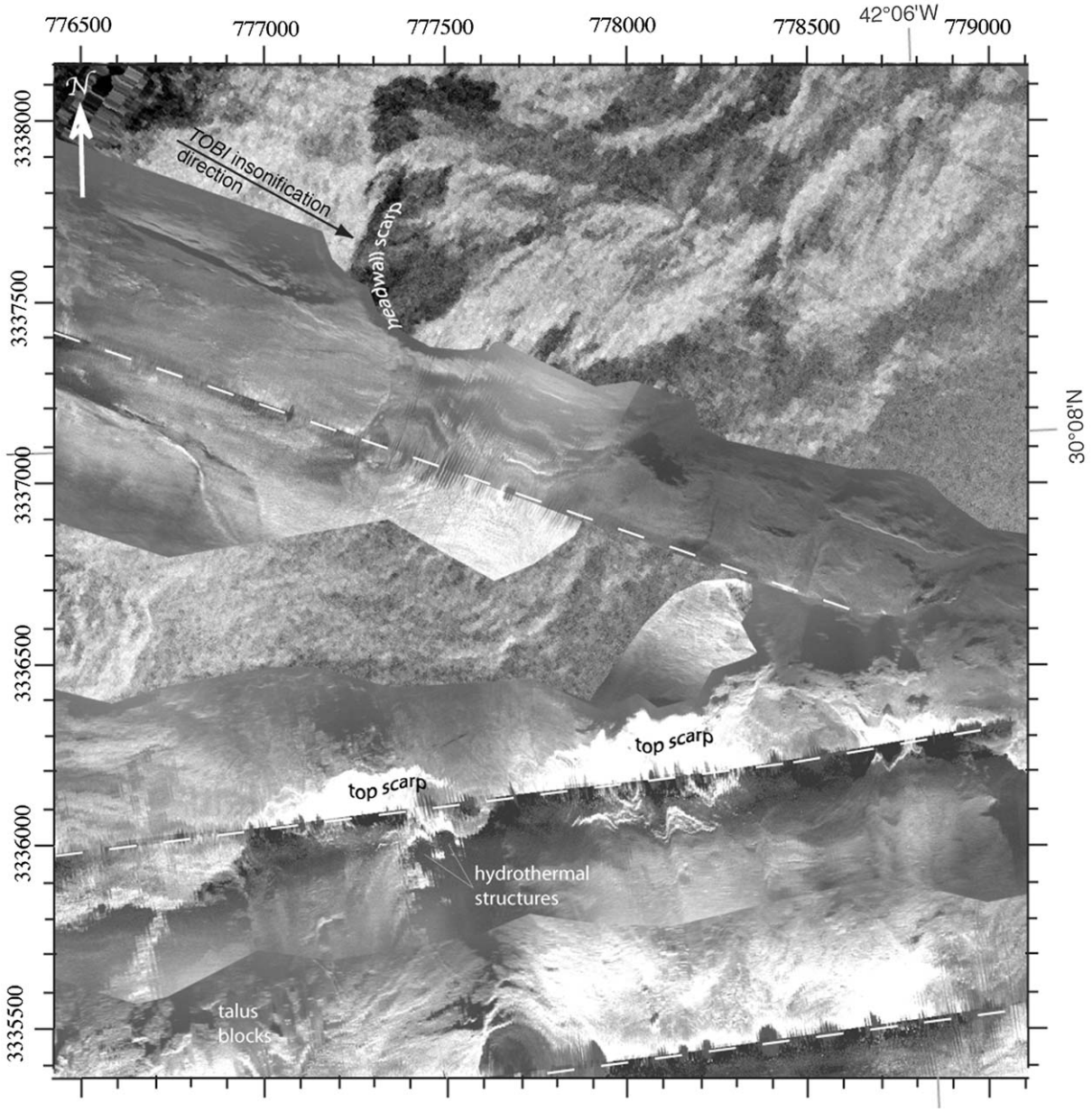

Figure 8. Side-scan sonar image of the central part of the Southern Ridge. *DSL-120* swaths are overlain on *TOBI* data (location shown in Figure 3). Dashed white line shows center of *DSL-120* tracks which have some portions cut away so that features in *TOBI* data are visible. Difficulties with seafloor detection on the steep slopes below the top scarp results in numerous artifacts near the *DSL-120* centerline (nadir). The top of the ridge has continuous, smooth backscatter characteristic of pelagic sediment. Note strong, arcuate reflectors and downslope-trending debris chutes along the top of the South Wall. The Lost City hydrothermal vent field is located near the summit of the ridge at the top of the South Wall.

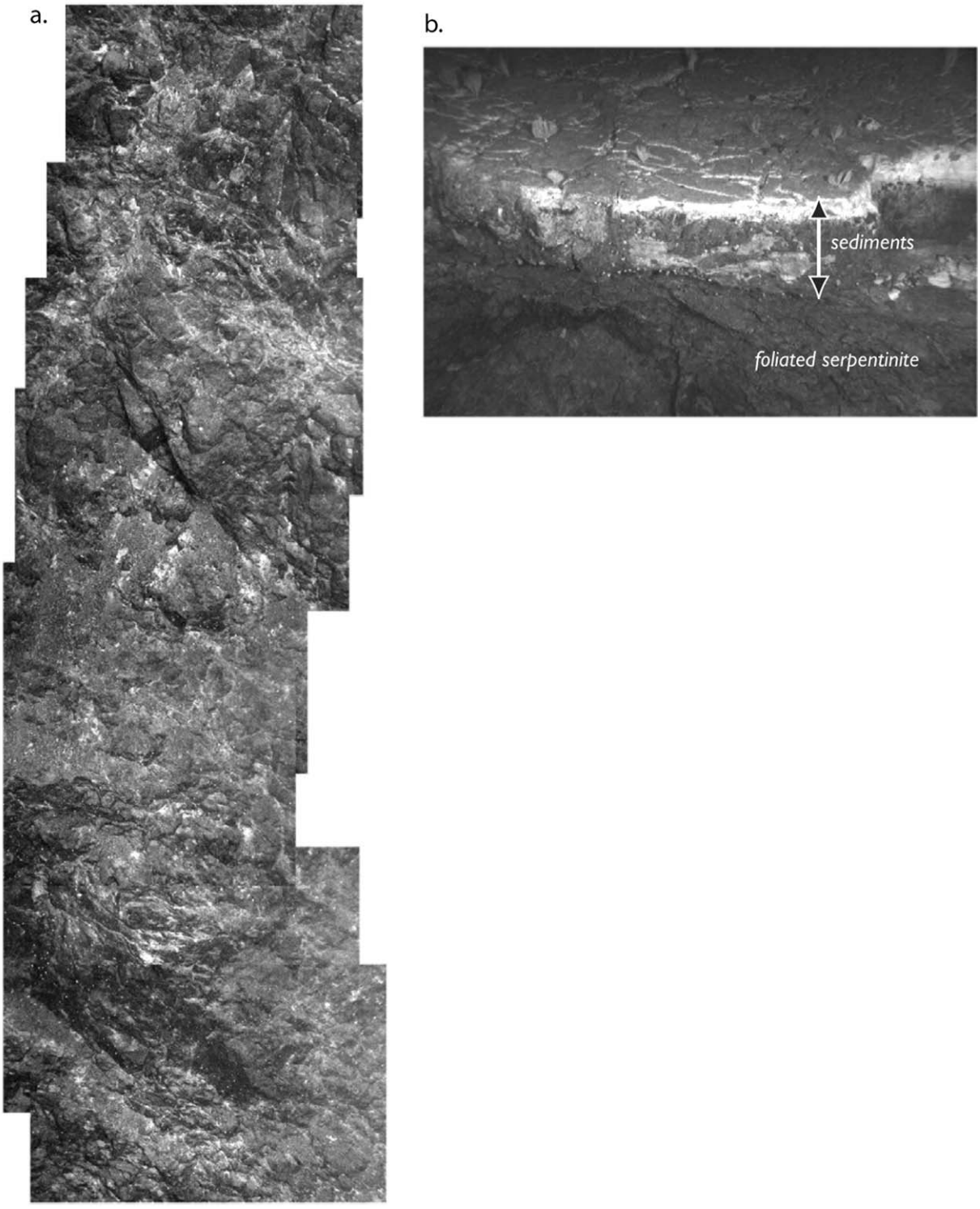

Figure 9. Imagery data from the South Wall of Atlantis Massif. a) Photomosaic of *DSC* images obtained during an *Argo II* survey (∼778200, 3336300, depth 904 m). This ∼40 m high image illustrates the structure within exposures of variably deformed serpentinites along the topmost scarp. View angle of the camera is 30˚ downward. b) A single *DSC* image illustrates the sedimentary units deposited unconformably on foliated serpentinite on the top of the South Wall. White chalk caps the sequence and cracks within it indicate the degree of induration. Corals are growing on top.

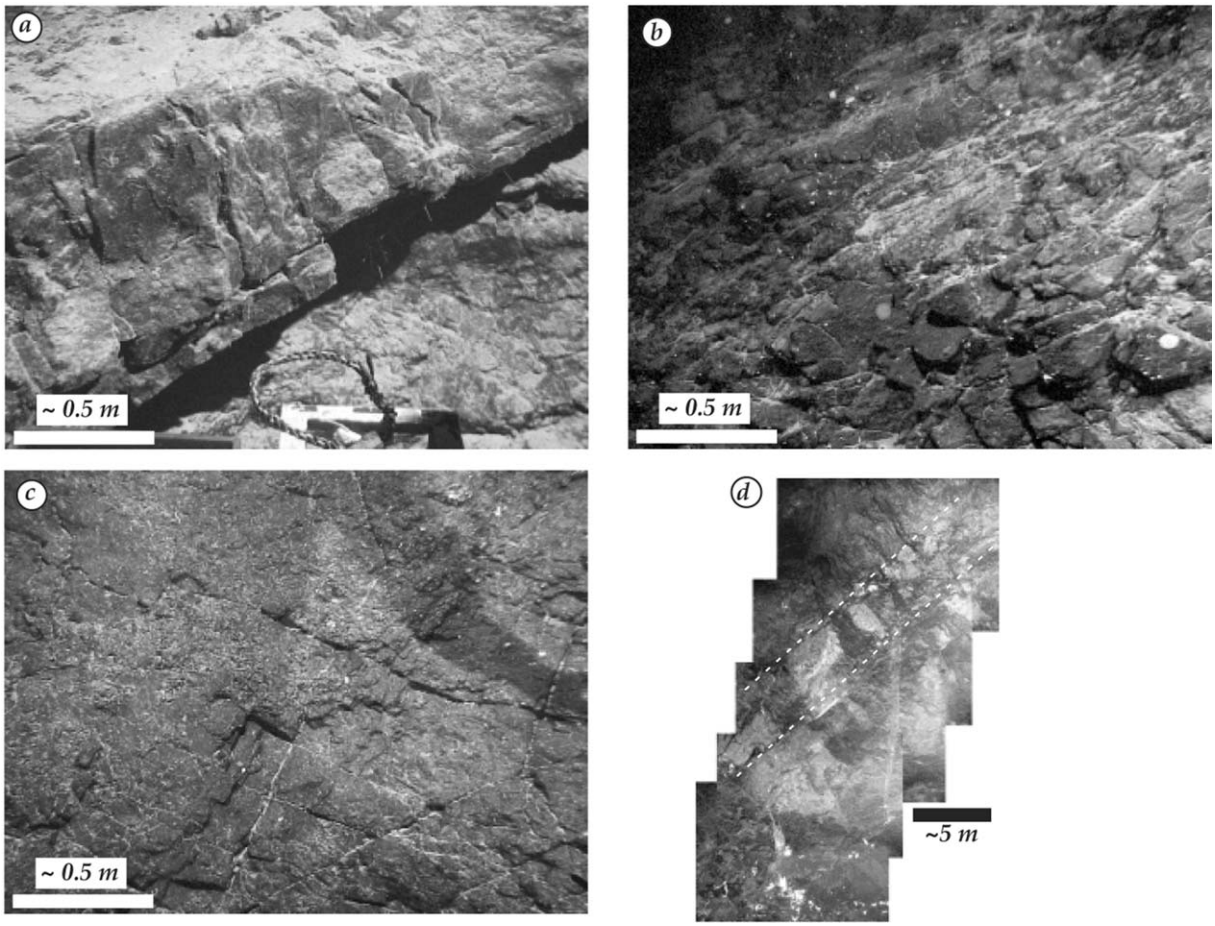

Figure 10. Basement outcrops on the South Wall of the massif. Handheld digital photographs from *Alvin* dives (location in Figure 2a) are shown in (a–c). (a) massive serpentinite, (Dive 3650, 3000 m); (b) serpentinite with anastomosing foliation (Dive 3645, 1270 m); (c) massive outcrop typical of metagabbbro (Dive 3645, 983 m); (d) cross-jointed, basaltic dike (?), between dashed lines, cutting serpentinites. Mosaic of *DSC* images obtained during *Argo II* survey (~777600, 3336100, 840 m). Camera view angle is 30°.

common, as is low-temperature overprinting, seafloor weathering, and carbonate vein formation (Figure 11 a, f, i). One dike of rodingitized gabbro was sampled deep on the South Wall (Figure 2a, $x = 773800$, $y = 3330500$).

In several outcrops along the top of the South Wall, breccias with carbonate matrix unconformably overlie foliated serpentinite (Figure 9), and carbonate veins and open fissures partially filled with delicate, finger-like growths of carbonate are visible. Some samples show a complex array of cross-cutting, variably deformed serpentine and carbonate veins (Figure 11f) that are reminiscent of those found in Alpine ophicalcites (Weissert and Bernoulli, 1985; Lemoine et al., 1987; Früh-Green et al., 1990; Treves and Harper, 1994; Treves et al., 1995). Some deformed veins contain microfossils indicating that the fractures were open to the surface during deformation of the host serpentinite (Schroeder et al., 2002).

Microstructural analysis shows that the rocks were subjected to shear deformation and dilational fracturing at metamorphic conditions ranging from granulite to sub-greenschist facies. High temperature (>700 °C), ductile deformation of both gabbro and peridotite is dominated by crystal plastic flow and formation of mylonitic shear zones, where grain size reduction by dynamic recrystallization is characteristic (Figure 11j, k; Schroeder et al., 2001). Rocks from all structural levels sampled on the South Wall display strong ductile deformation.

Ductile deformation fabrics in peridotite samples are overprinted by semi-brittle and brittle deformation (Figure 11h), which indicates that shear strain was accommodated by cataclasis and diffusive mass

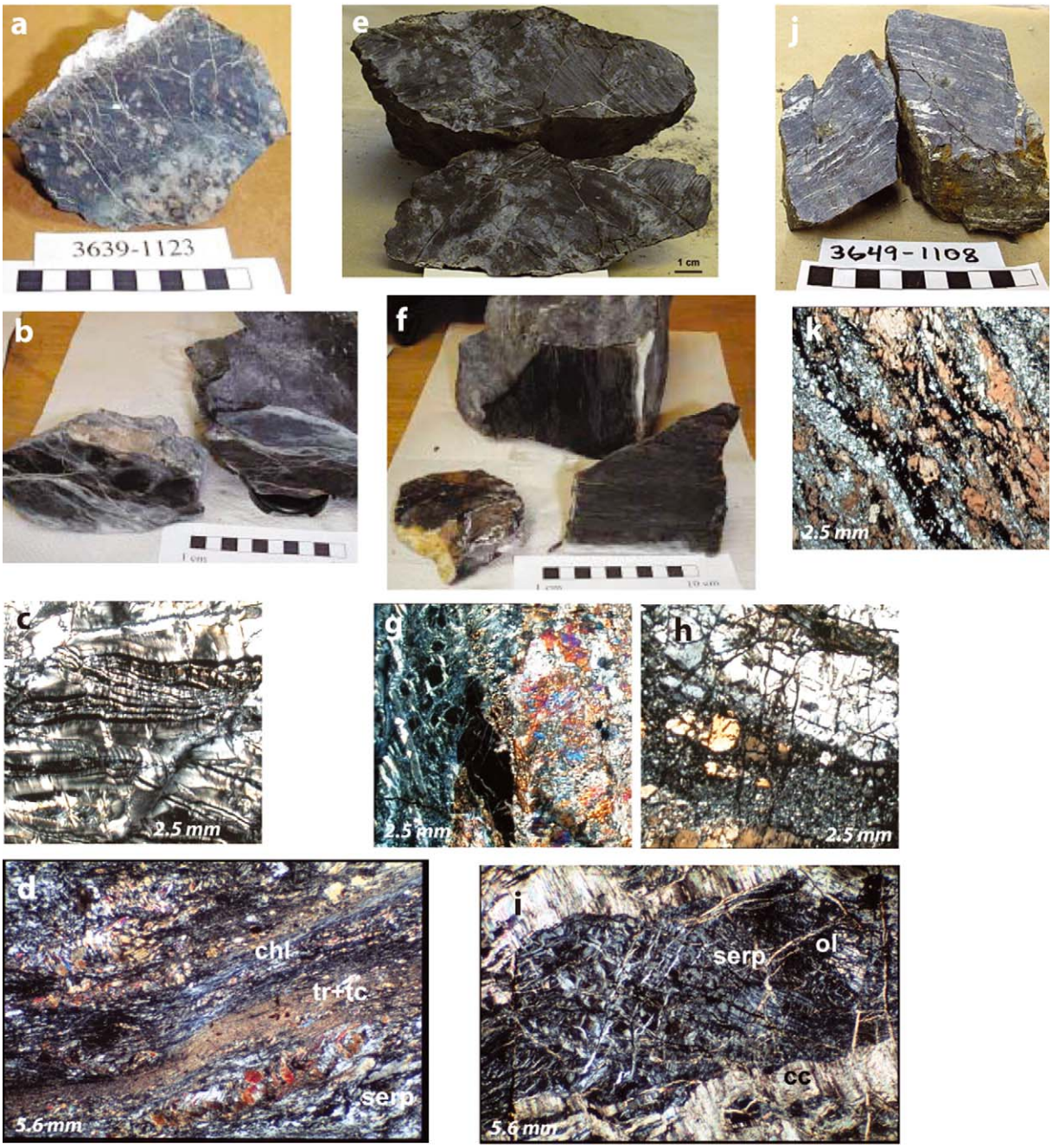

Figure 11. Rock samples from the South Wall of Atlantis Massif. Scale bar in hand sample photos is 10 cm. Size of each photomicrograph is labeled. (a) Typical serpentinite, Dive 3639, 1550 m. (b) Foliated serpentinite, Dive 3639, 1475 m. (c) Ribbon textured serpentinite. Foliation is defined by parallel serpentinite and magnetite veins that parallel earlier-formed crystal plastic fabric. Dive 3648, 947 m. (d) Sheared serpentinite with fine-grained domains consisting of parallel oriented tremolite (tr), talc (tc) and chlorite (chl). Dive 3639, 1472 m. (e) Highly serpentinized peridotite cut by gabbroic vein. Primary textures in the vein are obliterated by pervasive alteration to tremolite, talc, and chlorite. Dive 3652, 884 m. (f) Deformed carbonate veins in serpentinite, Dive 3639, 1475 m. (g) Margin of highly altered vein in serpentinite. Vein is dominantly tremolite with minor talc and chlorite cutting kernel texture serpentinite. Dredge 3, ~783200, 3335100. (h) Margin of narrow amphibole-grade shear zone in metagabbro with weak brittle overprint. Finely recrystallized plagioclase and porphyroclasts are cut by minor-offset brittle fractures. Dive 3652, 874 m. (i) Highly serpentinized peridotite cut by a dense network of calcite-filled veins (cc). Calcite veins have kink bands and cut earlier serpentine (serp) mesh textures and veinlets. Relict olivine (ol) texture is partially preserved in spite of high degree of alteration. Dive 3652, 863 m. (j) Deformed metagabbro. Dive 3649, 1423 m. (k) Amphibolite-facies metagabbro mylonite with segregated bands of recrystallized plagioclase, brown hornblende and Fe-Ti oxide. Plagioclase is deformed by crystal plastic flow with minor cataclasis. Recrystallized grains of plagioclase range in size from 10–100 mm. From sample shown in (j).

transfer (Schroeder and John, 2002). Stable mineral assemblages of tremolite, chlorite and chrysotile indicate that the latter processes occurred at temperature less than 400 °C. Schroeder (2003) determines that it is less common for gabbroic samples to display deformation characteristic of the 200–400° temperature range, suggesting that reaction-weakening of peridotite by serpentinization and greenschist facies alteration promotes partitioning of strain away from the relatively stronger gabbro (Schroeder et al., 2001). The occurrence of cataclastic deformation in samples at from a range of structural depths indicates that a series of faults have been active as Atlantis Massif evolved.

Because the top of the corrugated Central Dome had previously been interpreted as a detachment fault and at least the eastern part of the Southern Ridge has similar surface features, we anticipated finding a discrete, low-angle fault zone at the top of the South Wall. Photomosaics from five nights of *Argo II* surveying (Figure 2a) do not show consistent outcrop structure that might document a single, major fault zone along the top of the southernmost scarps. Three *Alvin* dives (3645, 3651, and 3652, from west to east as shown in Figure 2a) reached the very top of the South Wall. The easternmost of these dives (3652) crossed the summit in two transects, laterally offset by ∼800 m. In both of these crossings, subhorizontal, parallel fracturing was observed in outcrops within the top ∼100 m section just beneath a breccia/carbonate unit that caps the summit of the massif. In contrast, the western crossing of the summit (Dive 3645) did not encounter such outcrop structure near the summit. Microstructural analysis of samples from both dives indicates that brittle deformation is concentrated in a section that occurs within the 50 m section just below the sedimentary cap units. This limited finding may be bolstered by microstructural analyses of the full suite of ultramafic south wall dive samples, although an assumption about the prior depth of the corrugated surface is required in the areas where extensive landslides have probably removed portions of it. Schroeder (2003) defines a projection of the domal surface extending west from the actual corrugated surface on the Southeast Shoulder. He determines that almost all samples that display a high degree of brittle deformation occur at a structural depth, defined below the (partly assumed) surface, of less than ∼50 m (Schroeder and John, 2002; Schroeder, 2003).

Along the South Wall, talus slopes extending hundreds of meters downslope are common, hosting angular gravel- to cobble-size fragments. Rarely, very large (tens of meters across) intact blocks are included. The immense blocks are also visible in the side-scan images (Figure 8).

The Southern Ridge. The Southern Ridge is 3–5 km wide and its transform-parallel length is about 15 km. Surface corrugations and striations are less prominent than those that typify the Central Dome, and the Southwest Shoulder lacks these features altogether. The ∼7 km^2 summit area of the ridge averages about 750 m depth and the *DSL-120* bathymetry data indicate that the peak itself is elongate in the NS direction. A large, arcuate scarp cuts into the NE side of the summit (break in slope $x = 777200$, $y = 3337500$, Figures 3 and 8) and bounds a 1.5-km-wide, downslope-trending depression extending ∼2 km to the NE. The scarp defines the NE edge of the top of the peak, and appears to be the headwall scarp of a large mass-wasting feature.

Striations on the Southern Ridge are visible up to 3 km west (Figure 8) of the summit area and 5 km to the east (Figure 12). The lateral extent of the striations is similar to that of the Central Dome, but the area where they occur lies 2–3 km farther to the east. The southeast shoulder of the ridge displays striations and poorly defined corrugations on an area that extends 2 to 3 km south of the summit. The nature and extent of these lineaments indicate that at least the eastern portion of the Southern Ridge was affected by the same processes that created the corrugated and striated Central Dome.

A steep scarp truncates the southeast shoulder of the Southern Ridge, with NNE-trend and ∼40° dip toward the RTI (Figure 12). Just beyond the northern end of the scarp, pillow basalt up to several tens of meters thick was observed during an *Argo II* run (Figure 2a). However, most of the top and eastern portion of the scarp are covered by sediment and rubble produced by mass wasting. An *Alvin* dive (3647) on the eastern slope of the southeast shoulder crossed some basement, but mostly rock debris that included blocks up to at least 10 m across. In this area, active debris chutes and talus ramps cut into and bury older slides. Samples collected here include a wide range of metagabbroic rocks that exhibit complex overprinting of metamorphic mineral assemblages and veins, in addition to a few basalts (Figure 2a, online supplement Table I).

The western shoulder of the Southern Ridge has a distinctly different acoustic signature than the eastern shoulder (Figure 13). No striations are visible

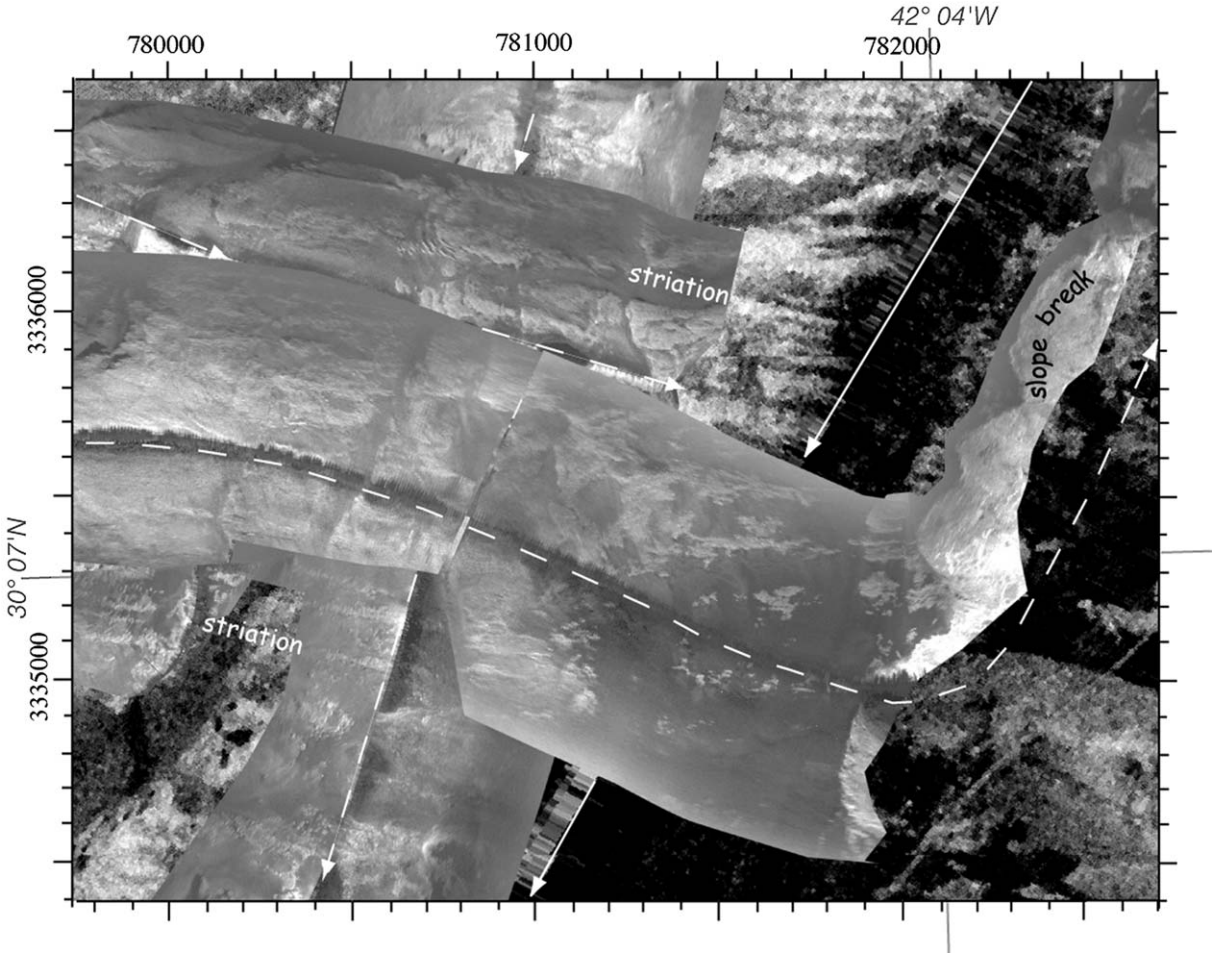

Figure 12. Side-scan sonar image of the eastern part of the Southern Ridge (southeast shoulder). *DSL-120* side-scan swaths are overlain on *TOBI* data (location in Figure 3). Solid white line indicates TOBI track centerline. dashed white line shows *DSL-120* track centerline, to clarify insonification directions where portions of image are cut away. Distinct, ESE-trending striations occur in this area, suggesting that it may be related to the Central Dome although these southern striae are coarser. Note the sharp scarp edge to the southeast.

and bright reflectors with diverse acoustic textures are present in patches. Locally, these areas are cut by dark 'channels' (e.g. $x = 772000$, $y = 3338300$, Figure 13) that extend for hundreds of meters and trend in several different directions. Low-acoustic-backscatter areas occur in some places but not as extensively nor in such large fields as elsewhere on the massif. Based on the sharpness and shape of the dark/bright backscatter boundaries, many low-backscatter areas appear to be shadows associated with locally rough topography. Other dark areas are interpreted as sediment ponds.

At the top of the South Wall, variably foliated to massive serpentinites are unconformably overlain by a distinctive sequence of flat-lying sedimentary deposits including breccias, chalk, and variably consolidated carbonate ooze (Figure 9). The contact between the serpentinites and the sedimentary rocks is sharp, but gently undulating locally in some outcrops, with a few meters of relief. It is clearly a depositional contact. The smooth upper surface of the sedimentary sequence is the seafloor, which has a gentle slope up toward the crest of the Southern Ridge. Only minor, local, erosional features disturb the sedimentary sequence. The general absence of bright reflectors in the side-scan sonar images from the top of the central and eastern Southern Ridge likely indicates that this smooth sediment surface blankets much of the area.

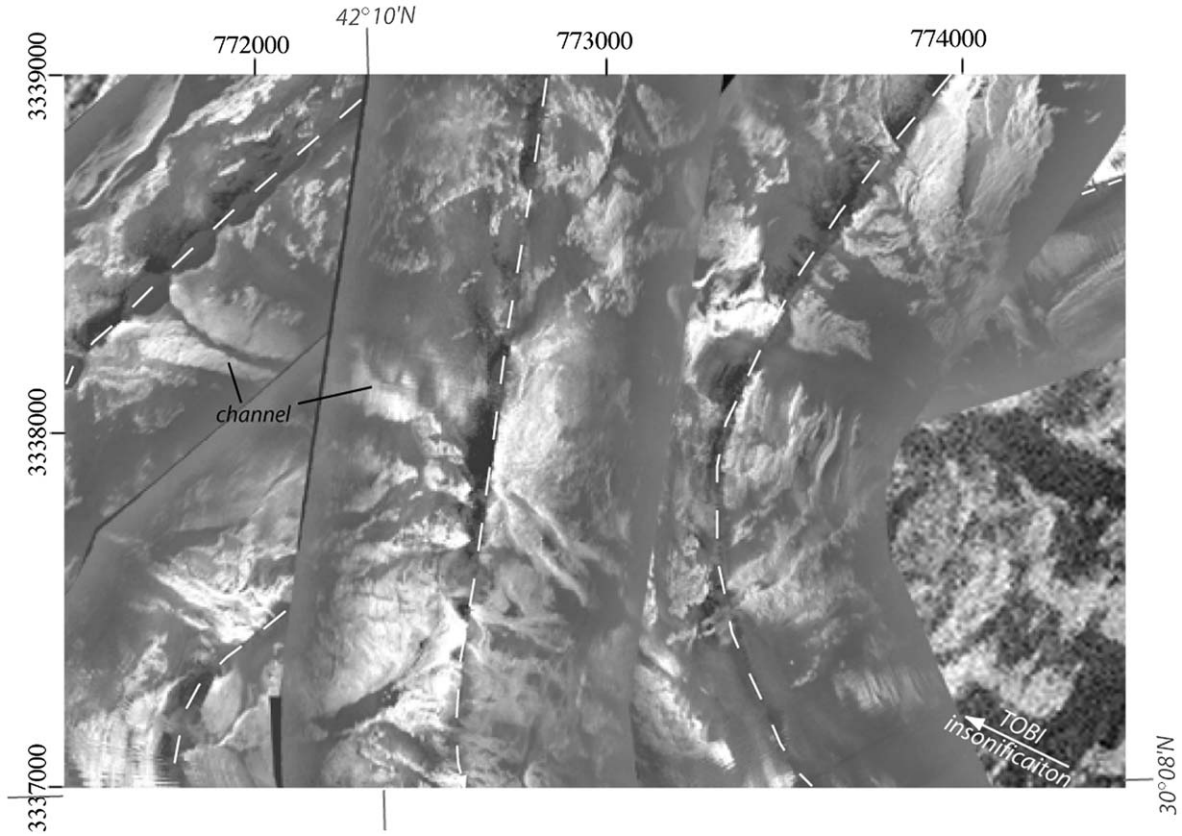

Figure 13. Side-scan sonar image of the western side of the massif. *DSL-120* side-scan overlain on *TOBI* data (location in Figure 3). Dashed white line shows *DSL-120* centerline. Note patches of linear and irregular reflectors (basement outcrops?) and large areas of low backscatter (sediment covered areas). Smooth, downslope-trending swaths are probably channels produced by mass wasting.

Summary and Interpretation

Integration of the MARVEL results with data from previous studies shows that the Atlantis Massif has experienced a complex tectonic and hydrothermal activity. Both processes probably contributed to uplift of the massif as well as influencing its ongoing morphological evolution. The time period over which the tectonism and hydrothermalism have occurred must be less than 2 Myr, although it could have been considerably less depending on when initial development of the massif began. The morphotectonic map in Figure 14 summarizes our current interpretation of the Atlantis Massif.

All available evidence indicates that the Eastern Block is a continuous block of variably fractured upper crustal material that lies between the top of the median valley wall and the corrugated Central Dome. However, because contacts with surrounding terranes are not exposed, there is no unique interpretation for how and when the Eastern Block formed with respect to other parts of the massif. It is likely that this block represents allochthonous upper crustal material, underneath from which the footwall has been transported WNW by several kilometers. The angular rubble fragments sampled from the Central Dome are mostly metabasalt whose metamorphic grade indicates alteration temperatures of 300 °C. The fragments could have broken off the underside of the now-displaced hanging wall to the east. However, it is also possible that the Eastern Block basalt was erupted in contact with the corrugated surface on the median valley floor and that the Eastern Block has been elevated while in contact with the detachment fault surface. In this case the metabasalts would have to be relicts of the underside of a hangingwall block now buried beneath the Eastern Block. Rare features interpreted as intact volcanic cones on the eastern slope of the Central Dome indicate that at least some volcanism occurred on the corrugated surface. The backscatter character-

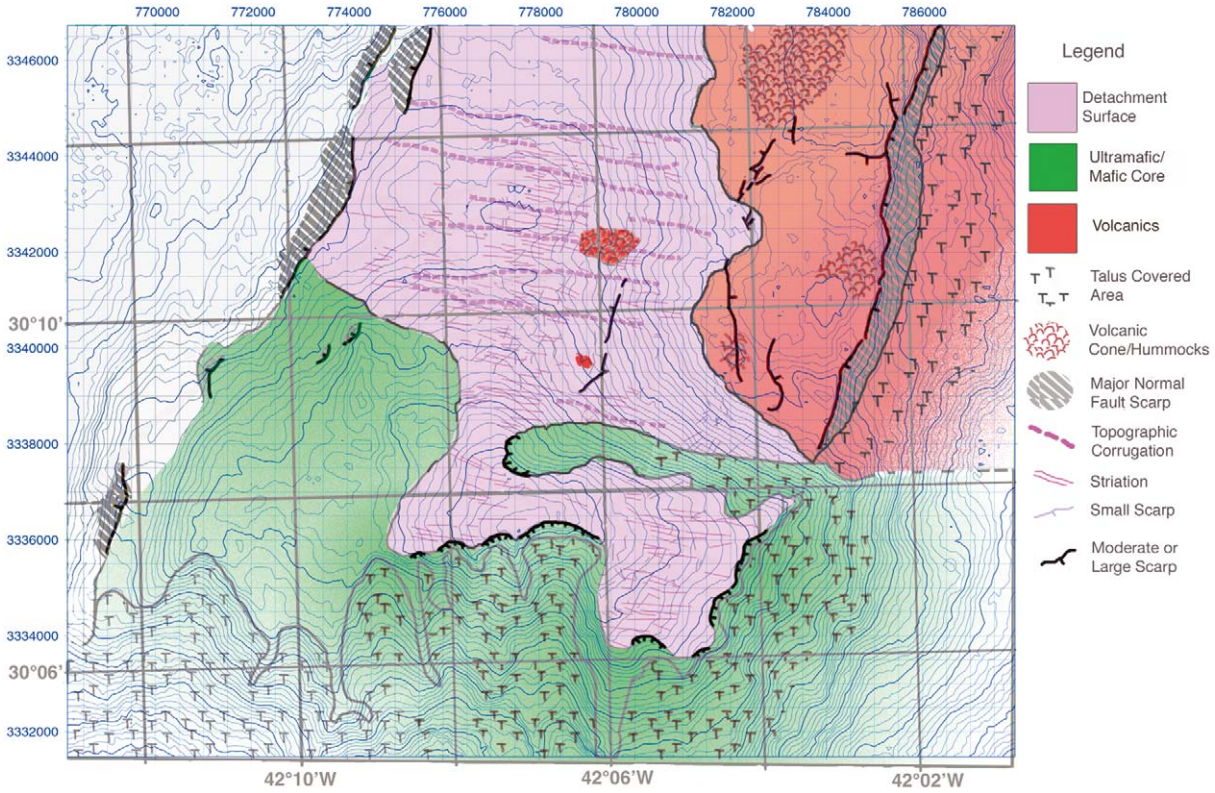

Figure 14. Morphotectonic map of Atlantis Massif based on sidescan sonar, basic rock type distribution, *Alvin* dive mapping, *Argo II* video imagery and bathymetric data. The MAR median valley is just off the right side of the map and the Atlantis transform fault is off the bottom of the map. Blue contours are at intervals of 50 m with heavy contours every 250 m, the shallowest of which is 1000 m. This oceanic core complex exposes rubble-covered detachment surfaces that cap foliated, serpentinized peridotite and lesser metagabbroic rock within the core. The eastern basaltic block is interpreted to be an upper crustal hanging wall block.

istics of these features indicate that they are covered with sediment so are probably not recently erupted.

Despite the distinctive and compelling nature of the corrugations and striations on the Central Dome, determining their geologic cause using seafloor mapping is challenging because basement outcrops are very scarce on the surface of the massif. Outcrop mapping along of the top of the eastern South Wall and deformation in samples from several areas along the uppermost scarp indicates that a major fault caps at least portions of the Southern Ridge.

The patterns of striations observed in the *DSL-120* side-scan sonar are not as regular as previously inferred from *TOBI* data. Locally, areas of more complex curvilinear striations are reminiscent of outcrop patterns on erosional surfaces in complexly deformed continental basement terranes. These patterns tend to occur on surfaces that are exposed at greater water depths and may represent tectonic or erosional exposure of structurally deeper material, perhaps the basement beneath a pre-existing, regularly striated detachment exposure. For example, if the Southern Ridge at one time was completely capped with a corrugated surface, the current Southwest Shoulder might represent such an exposure of basement from underneath the now-removed surface.

Minor gabbroic outcrops do not display an obvious preferred orientation or spatial distribution, although all samples from these exposures are deformed. High-temperature (granulite to amphibolite facies) mineral assemblages in gneissic to mylonitic metagabbros (Kelley et al., 2001; Schroeder et al., 2001) indicate that at least locally intense deformation must have occurred at significant subseafloor depths. Overprinting lower-temperature, brittle features may have been acquired during partial serpentinization and shearing of the surrounding peridotites (Boschi et al., 2002; Früh-Green et al., 2001; Schroeder et al., 2001, 2002). Stable isotope data and the mineral assemblages in the serpentinized peridotites indicate that much of the

serpentinization and metasomatism occurred at temperature of approximately 200–400 °C (Früh-Green et al., 2002).

Field observations and sampling on the South Wall indicate that this area is dominated by variably deformed and highly altered serpentinite, with lesser metagabbro. However, seismic data indicate that anhydrous peridotite (seismic velocity >8 km/s) occurs at depths of less than a kilometer below the surface of the Central Dome (Detrick and Collins, 1998; Collins et al., 2001). Thus, the exposures on the South Wall may represent a thin veneer of altered rock. Alternatively, because most of our coverage of the South Wall is located where it cuts deeply into the interior of the Southern Ridge and the slope failure could have occurred relatively recently, the findings may indicate that serpentinization penetrated to greater depth there than at the Central Dome. Gravity data (Blackman et al., 1998) show that much of the Southeast Shoulder is underlain by high-density material (3100–3200 kg/m^3, if surrounding crust averages 2850–2900 kg/m^3), similar to that beneath the eastern slope of the Central Dome (Figure 15). In addition, the lower slopes of the central part of the South Wall must be underlain by high-density, presumably less extensively altered rock, based on the gravity high in that area. In contrast, most of the summit area of the Southern Ridge, and a central area, ~2 km wide, on the Southeast Shoulder are characterized by gravity anomalies up to 5 mGals lower than the highs associated with the rest of the core of the complex. These relative gravity lows may reflect density reduced by serpentinization at depth. If this is the case, the uplift of the Southern Ridge may have been enhanced, relative to the Central Dome, by significant volumetric expansion associated with serpentinization (O'Hanley, 1996). Venting of high pH fluids at the Lost City Hydrothermal Field demonstrates that serpentinization is still ongoing, with outflow focused near the summit of the Southern Ridge (Kelley et al., 2001).

Striations and corrugations, similar to those of the Central Dome, occur on the eastern part of the Southern Ridge. One possibility is that the top of the Southern Ridge is an uplifted surface that was once continuous with that of the Central Dome. Uplift may have been responsible for arresting the spreading-parallel displacement along the southern portion of the detachment. Continued displacement to the north would have resulted in the several-kilometer westward step in the position of the Central Dome relative to the corrugated, striated portion of the Southern Ridge. In this scenario, there never would have been a corrugated surface over the current Southwest Shoulder. There does not appear to be a distinct break in the corrugated surface between the Central Dome and that on the Southern Ridge. If the evolution of the two parts of the detachment did differ, a means of enabling their separate behavior must exist somewhere to the north of the Southeast Shoulder. Strands of any transfer zone (Karson, 1992) that might accommodate the offset along the steep northern side of the Southeast Shoulder are not visible in our sidescan data, although high-resolution coverage is not continuous in this area. The landslide marked by a headwall scarp on the northeast side of the summit peak, and debris that extends several km to the east (Figures 3, 8, and 14), may document tectonic activity along such a zone. The sections of pillow basalt observed at the very top of the northern slope on the Southeast Shoulder could be bits of the hanging wall block, uplifted during the rise of the Southern Ridge.

Discussion

One of the defining characteristics of dome-like seafloor massifs of OCC is their smoothly arched, corrugated and striated upper surface. These surfaces are interpreted to expose major detachment faults with spreading parallel displacements comparable to the width of the massifs. At up to 20 km, this corresponds to as much as 2 Myr of focused slip on Atlantic detachment faults (Tucholke et al., 1998). The thickness of the Atlantic detachment zones appears to be of the same order as continental detachments- many tens to a hundred meters. Seafloor determinations are generally more difficult than subaerial mapping due to logistical limitations but several dives at Atlantis Massif (subsection on The South Wall), drilling during Ocean Drilling Program Leg 153 in the MARK area, 23° N MAR (Karson and Dick, 1983; Gillis et al., 1993; Karson and Lawrence, 1997), and rock drill work and targeted dredging on the 15° 45′ N (MacLeod et al., 2002; Escartin et al., 2003) all indicate detachment zone thickness of several tens of meters. Submersible mapping and sampling on the flanks of Atlantis Bank, SWIR (Miranda et al., 2002) suggest that parts of that detachment system contains slip zones up to 500 m thick.

At the Atlantis Massif, the composition and deformation are heterogeneous with depth along the South Wall. Sheared serpentinites with intervening

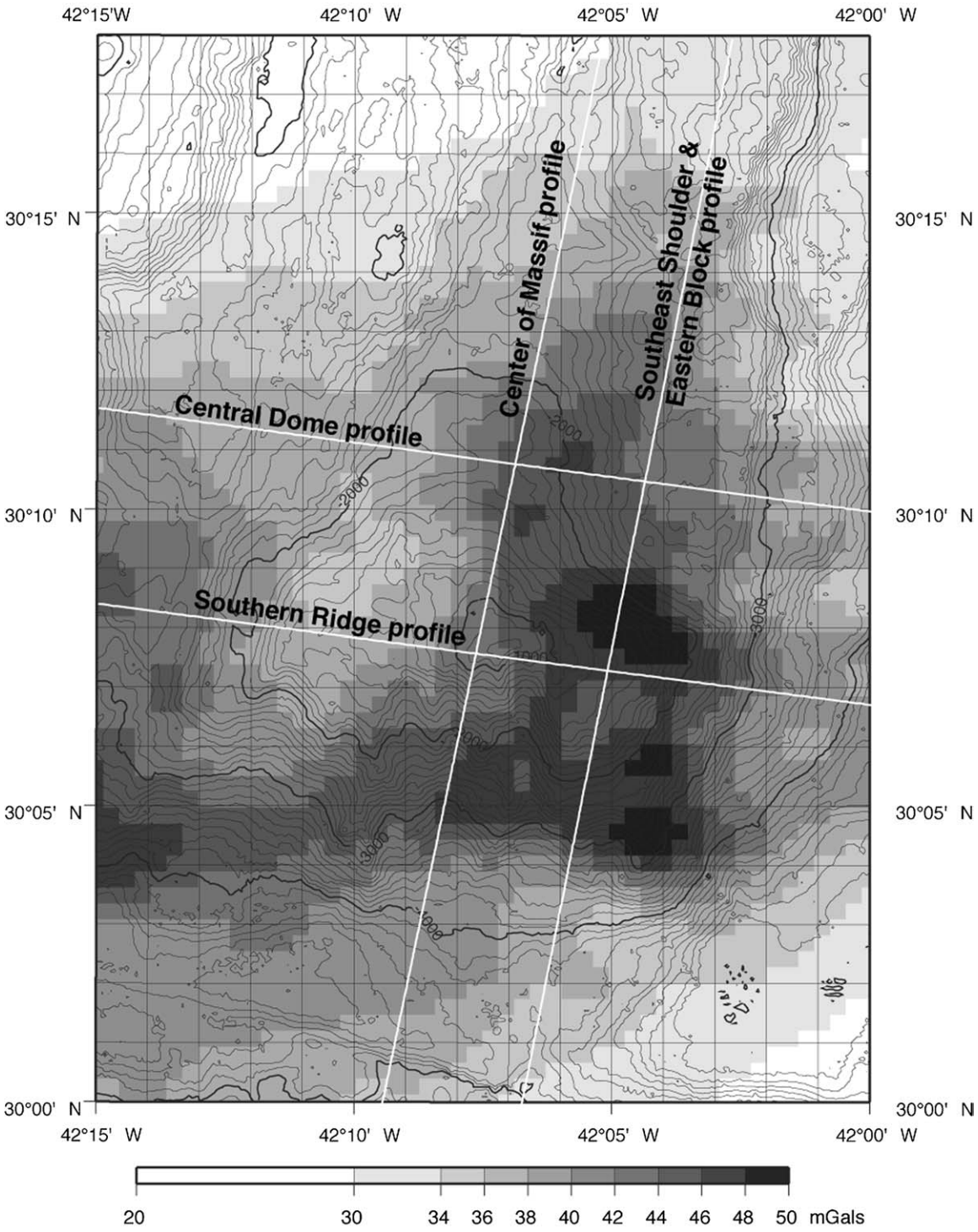

Figure 15. Residual gravity anomalies (grayshade) at Atlantis Massif; contours show topography at 100 m interval. Contribution of seafloor topography has been removed from the Free Air Anomaly, as has a model of constant thickness, constant density crust. A model of density increase associated with simple lithospheric cooling has also been removed to obtain this residual gravity anomaly map (from Blackman et al., 1998). Location of profiles in Figure 16 are shown and labeled.

bodies of more massive serpentinite occur throughout a 2500 m thick interval from the top. No consistent relationship has been discerned between these rocks and the intercalated, less common gabbros. Similarly, a variable distribution of deformation fabric is documented for seafloor samples from ultramafic exposures at the MAR axis near the 15° 20′ N fracture zone (Cannat et al., 1997). Such variable distribution of deformation with depth in the core of oceanic complexes likely indicates that extension was distributed between a series of faults (a detachment system), similar to that documented in continental core complexes (John, 1987).

Relative lows in the gravity anomaly map indicate that the depth to which serpentinization penetrates varies within and between the Southern Ridge and the Central Dome (Figure 15). This variation is probably controlled by the distribution of faults and fracturing that are secondary, relative to the detachment. Steep faults that strike parallel to the southern edge of the massif and to the ATF significantly enhance permeability in this area. Intense fracturing along this part of the massif also includes a network of ∼NS features and likely promotes hydrothermal circulation and hence serpentinization.

Cross sections (Figure 16) illustrate the type of variability that occurs within the core of the Atlantis Massif and the possible relationships of adjacent blocks. The schematic sections are constrained by a series of 2-D gravity models in which the density contrast and shape of subsurface bodies was varied to determine the limits of structure that match the observed gravity profiles to within the 2 mGal accuracy (Blackman et al., 1998) of the seasurface data. The 2-D models provide a useful guide for geologic inference. Future, more detailed assessment will require a 3-D gravity modeling approach due to the complexity of the structure and the topograhic relief of the area (Parker, 1995; Nooner et al., 2003).

There appear to be differences in the depth to which serpentinization significantly lowers the density of the rock and these occur over lateral distances of 3–5 km. The alteration within portions of the Southern Ridge may extend 500–1000 m deeper than that beneath the Central Dome, particularly in the summit area. Buoyancy forces associated with volumetric expansion that accompanies serpentinization may also contribute to uplift of the domal core. The greater extent of serpentinization within the Southern Ridge may explain why the summit there achieved such shallow depths. Another factor in the greater uplift of the Southern Ridge may be its proximity to the transform fault that may act to decouple the corner of the plate from typical lithospheric stresses.

Based on the morphology and geological relations of the Atlantis Massif we infer a dramatic history of vertical uplift. The peridotite that makes up the core of the massif originated in the mantle within less than ∼15 km of the spreading axis, possibly below the axial valley itself. The depth at which this material was incorporated into the lithosphere is not known, nor is it clear how much overlying material might have been removed tectonically. The depth of the MAR median valley in this area is ∼4000 m, typical of many areas near slow-spreading RTIs (Purdy et al., 1991). The Central Dome of the massif is presently at an average depth of about 1800 m. Therefore, this region must have been uplifted at least 2200 m during incorporation into the western flank of the MAR. This uplift occurred in about 1.5 Myr yielding an uplift rate of ∼1.5 mm-yr^{-1}. The Southern Ridge has had additional uplift, totaling up to 4000 m, over a similar time span. The uplift history of the Atlantis Massif is extraordinary, but it may be typical of OCC. For example, topographic highs along the St. Paul, Romanche, and Vema fracture zones in the Atlantic probably formed at similar, inside corner settings and their uplift was even greater, they reached sea level before subsequently subsiding (Bonatti, 1978). The Atlantis Bank on the SWIR, a gabbroic core complex associated with partially serpentinized peridotite, has a beveled upper surface that was probably eroded at or near sea level (Dick et al., 2000).

Finally, the very sparse evidence of magmatic activity within the core of Atlantis Massif would, at first glance, suggest the validity of early hypotheses (Karson, 1990; Tucholke and Lin, 1994) that correlate a period of amagmatic spreading with the formation of the OCC in this area. The question arises, however, as to whether the current distribution of basaltic and gabbroic rocks within 20 km of the MAR-ATF RTI really supports this conclusion. Imbricate hanging wall blocks in the central part of the OCC may combine to ∼2 km thick magmatic section, at least a portion of which is envisioned to have once resided above the footwall. Regional gravity analysis (Pariso et al., 1996) shows that the Mantle Bouguer anomaly over the outside corner is 20–25 mGals lower than that over inside corner. This corresponds to a crustal section on the order of 2 km greater in thickness. The 7 km thickness determined for the outside corner (Pariso et al., 1996) is on the high end for Atlantic crust,

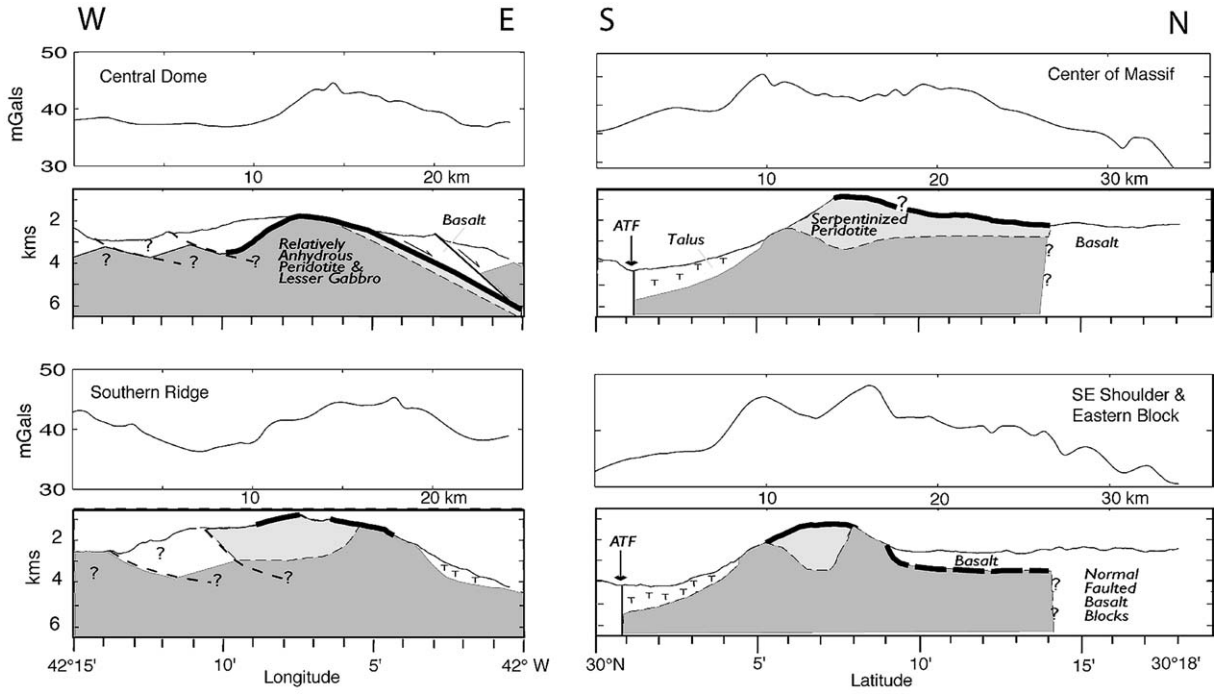

Figure 16. Schematic cross sections of the Atlantis Massif oceanic core complex. Profiles of bathymetry and residual gravity (Figure 15) illustrate the Central Dome, Eastern Block, and Southern Ridge areas in across-axis (panels on left) and along-strike (panels on right) views. Heaviest line shows detachment fault. Dashed heavy lines indicates possible normal fault. Gray shade indicates higher density material with light gray indicating density 100–150 kg/m^3 less than dark gray. White indicates lower density material. Structure and lithology in the west is conjectural but attempts to generally match the residual gravity anomaly.

particularly at the end of a segment. It is likely that asymmetric faulting of the crust (Karson, 1999) resulted in most of the magmatic section being spread to the eastern MAR flank while the lowermost crust and upper mantle section preferentially spread to the west. Canales et al. (2002, submitted) report that reflection seismic data indicate Layer 2A thickness and structure on the outside corner as typical to somewhat thick for Atlantic crust. More detailed geophysical and petrological data will be required to constrain the (east flank) lower crustal structure and the relationship between (west flank) footwall peridotites and outside corner basalts before a more confident conclusion can be drawn.

Acknowledgements

This project was supported by NSF Grants OCE 9712164 to D. Blackman, OCE9712430 to J. Karson, and OCE 9712549 to D. Kelley. In addition to the coauthors, B. Applegate, N. Bacher, H. Hanna, S. Lyons, P. Rivizzigno, and G. Sasagawa participated in the cruise and contributed to the data collection and onboard analysis. We thank the officers and crew of R/V Atlantis, the WHOI Deep Submergence Laboratory group who operated the *DSL-120* side-scan system and *Argo II*, and the *Alvin* Group for their outstanding effort in this challenging seafloor terrain. We also thank Dana Himmel for help with digital mosaics. Two anonymous reviewers contributed many useful suggestions for improving the presentation of results.

References

Blackman, D.K., Cann, J.R., Janssen, B. and Smith, D.K., 1998, Origin of extensional core complexes: evidence from the Mid-Atlantic Ridge at Atlantis fracture zone, *J. Geophys. Res.* **103**, 21,315–21334.

Boschi, C., Frueh-Green, G.L. and Kelley, D.S., 2002, Serpentinization and carbonate precipitation at the Lost City Vent Field (30N, MAR). *Geochim. Cosmochim. Acta* **66**(15A), A94.

Bonatti, E., 1978, Vertical tectonism in oceanic fracture zones, *Earth Planet. Sci. Lett.* **37**, 369–379.

Buck, W.R., 1988, Flexural rotation of normal faults, *Tectonics* **7**, 959–973.

Canales, J.P. Collins, J. and Tucholke, B., 2003a, Multichannel seismic imaging of oceanic core complexes in the Mid-Atlantic Ridge, EUG/AGU Spring Meeting, EAE03-A-04465.

Canales, J.P., Tucholke, B.E. and Collins, J.A., 2003b, Seismic reflection imaging of a young megamullion: Atlantis Massif (Mid-Atlantic Ridge, 30° 10′ N), *Earth Planet. Sci. Lett*. submitted.

Cann, J.R., Blackman, D.K., Smith, D.K., McAllister, E., Janssen, B., Mello, S., Avgerinos, E., Pascoe, A.R. and Escartín, J., 1997, Corrugated slip surfaces formed at ridge-transform intersections on the Mid-Atlantic Ridge, *Nature* **385**, 329–332.

Cannat, M., Lagabrielle, Y., Coutures, N., Bougault, H., Casey, J., Dmitriev, L. and Fouquet, Y., 1997, Ultramafic and gabbroic exposures at the Mid-Atlantic Ridge: Geological mapping in the 15° N region, *Tectonophysics* **279**, 193–214.

Ceuleneer, G. and Cannat, M., 1997, High-temperature ductile deformation of Site 920 peridotites, in Karson, J.A., Cannat, M., Miller, D.J. and Elthon, D. (eds.), *Proc. ODP, Sci. Results* **153**, College Station, TX (Ocean Drilling Program), 23–34.

Collins, J.A., Tucholke, B.E., and Canales, J-P., 2001, Structure of Mid-Atlantic Ridge megamullions from seismic refraction experiments and multichannel seismic reflection profiling, *Eos Trans. AGU,* F1100.

Davis, G.A. and Lister, G.S., 1988, Detachment faulting in continental extension: perspectives from the southwestern U.S. Cordillera, *Geological Society of America, Special Paper* **218**, 133–159.

Detrick, R.S. and Collins, J.A., 1998, Seismic structure of ultramafics exposed at shallow crustal levels in the Mid-Atlantic Ridge rift valley at 15° N, *Eos, Tran. AGU*, F800.

Dick, H.J.B., 1989, Abyssal peridotites, very slow spreading ridges and ocean ridge magmatism, in Saunders, A.D., and Norry, M.J. *Magmatism in the Ocean Basins* (eds.), pp. 71–105, London.

Dick, H.J.B., Meyer, P., Bloomer, S., Kirby, S., Stakes, D. and Mawer, C., 1991, Lithostratigraphic evolution of an *in situ* section of oceanic layer 3, in Herzen, R.P.V. and Robinson, P.T. (eds.), *Proc. Ocean Drilling Program, Sci. Res.*, pp. 439–515, College Station, TX.

Dick, H.J.B., Natland, J.H., Alt, J.C., Bach, W., Bideau, D. and Gee, J.S., 2000, A long in situ section of the lower oceanic crust: results of ODP Leg 176 drilling at the Southwest Indian Ridge, *Earth Planet. Sci. Lett.* **179**, 31–51.

Escartín, J. and Cannat, M., 1999, Ultramafic exposures and the gravity signature of the lithosphere near the Fifteen-Twenty Fracture Zone (Mid-Atlantic Ridge, 14° –16.5° N), *Earth Planet. Sci. Lett.* **171**, 411–424.

Escartín, J., Mével, C., MacLeod, C.J. and McCaig, A.M., 2003, Constraints on deformation conditions and the origin of oceanic detachments: the Mid-Atlantic Ridge core complex at 15° 45′ N, *Gcubed.*

Früh-Green, G.L., Kelley, D.S., Bernasconie, S.M., J.A. Karson, Ludwig, K.A., Butterfield, D.A., Boschi, C. and Proskurowksi, G., 2003, 30,000 years of hydrothermal activity at the Lost City vent field, *Science* **301**, 495–498.

Früh-Green, G.L., Boschi, C., Kelley, D.S., Conolly, J.A. and Schrenk, M.O., 2002, The role of serpentinization in metasomatism, carbonate precipitation, and microbial activity: Stable isotope constraints from the Lost City Vent Field (MAR 30° N), *Eos, Trans. AGU*, Fall Meeting.

Früh-Green, G.L., Weissert, H. and Bernoulli, D., 1990, A multiple fluid history recorded in Alpine ophicalites, *J. Geol. Soc. London* **147**, 959–970.

Gillis, K.M., Thompson, G. and Kelley, D.S., 1993, A view of the lower crustal component of hydrothermal systems at the Mid-Atlantic Ridge, *J. Geophys. Res.* **98**, 19597–19619.

John, B.E., 1987, Geometry and evolution of a mid-crustal extensional fault system: Chemeheuvi Mountains, southeastern California, in Coward, M.P., Dewey, J.F. and Hancock, P.L. (eds.), *Continental Extension*, pp. 313–335.

John, B.E., Foster, D.A., Murphy, J.M., Fanning, C.M. and Copeland, P., 2002, Quantitative age and thermal history of in-situ lower oceanic crust – Atlantis Bank, SW Indian Ridge: *Interidge SWIR Workshop Proc.*, p. 42, Southampton, U.K.,

Karson, J.A., 1990, Seafloor spreading on the Mid-Atlantic Ridge: Implications for the structure of ophiolites and oceanic lithosphere produced in slow-spreading environments, in Malpas, J., Moores, E.M., Panayiotou, A. and Xenophontos, C. (eds.), Ophiolites and Oceanic Crustal Analogues: *Proceedings of the Symposium "Troodos 1987"*, pp. 125–130, Geological Survey Department, Nicosia, Cyprus.

Karson, J.A., 1992 Segment boundaries in oceanic and continental rifts; geometry and kinematics of transfer zones, *Eos, Transactions AGU* **73**, 286.

Karson, J.A., 1998, Internal structure of oceanic lithosphere: A perspective from tectonic windows, in Buck, W.R., Delaney, P.T., Karson, J.A. and Lagabrielle, Y. (eds.), *Faulting and Magmatism at Mid-Ocean Ridges*, pp. 177–218, American Geophysical Union, Washington, DC.

Karson, J.A., 1999, Geological investigation of a lineated massif at the Kane transform: Implications for oceanic core complexes, *Phil. Trans. Roy. Soc. Lond.* **357**, 713–740.

Karson, J.A. and Dick, H.J.B., 1983, Tectonics of ridge-transform intersections at the Kane Fracture Zone, 24° N on the Mid-Atlantic Ridge, *Marine Geophysical Res.* **6**, 51–98.

Karson, J.A. and Lawrence, R.M., 1997, Tectonic window into gabbroic rocks of the middle oceanic crust in the MARK area near Sites 921–924, in Karson, J.A., Cannat, M., Miller, D.J. and Elthon, D. (eds.), *Proceedings of the Ocean Drilling Program, Scientific Results*, pp. 61–76, Ocean Drilling Program, College Station, TX.

Kelley, D.S., 1997, Fluid evolution in slow-spreading environments, in Karson, J.A., Cannat, M., Miller, D.J. and Elthon, D. (eds.), *Proceedings of the Ocean Drilling Program, Scientific Results*, pp. 399–415, Ocean Drilling Program, College Station, TX.

Kelley, D.S., and Delaney, J.R., 1987, Two-phase separation and fracturing in mid-ocean ridge gabbros at temperatures greater than 700 °C, *Earth Planet. Sci. Lett.* **83**, 53–66.

Kelley, D.S., Gillis, K.M. and Thompson, G., 1993, Fluid evolution in submarine magma-hydrothermal systems at the Mid-Atlantic ridge, *J. Geophys. Res.* **98**, 19579–19596.

Kelley, D.S., Karson, J.A., Blackman, D.K., Früh-Green, G., Butterfield, D., Lilley, M., Olson, E.J., Schrenk, M.O., Roe, K.R., Lebon, J. and Shipboard Party, 2001, An off-axis hydrothermal vent field near the Mid-Atlantic Ridge at 30° N, *Nature* **412**, 145–149.

Lagabrielle, Y., Bideau, D., Cannat, M., Karson, J.A. and Mével, C., 1998, Ultramafic-mafic plutonic rock suites exposed along the Mid-Atlantic Ridge (10° N–30° N): Symmetrical-asymmetrical distribution and implications for seafloor spreading processes, in Buck, W.R., Delaney, P.T., Karson, J.A. and Lagabrielle, Y. (eds.), *Faulting and Magmatism at Mid-Ocean Ridges*, pp. 153–176, American Geophysical Union, Washington, DC.

Lavier, L., Buck, W.R. and Poliakov, A.N.B., 1999, Self-consistent rolling-hinge model for the evolution of large-offset low-angle normal faults, *Geology* **27**, 1127–1130.

Lemoine, M., Tricart, P. and Boillot, G., 1987, Ultramafic and gabbroic ocean floor of the Ligurian Tethys (Alps, Corsica, Appennines): In search of a genetic model. *Geology* **15**, 622–625.

MacLeod, C.J., Escartín, J., Banerji, D., Banks, G.J., Gleeson, M., Irving, D.H.B., McCaig, A.M., Niu, Y., Allerton, S. and Smith, D.K., 2002, First direct evidence for oceanic detachment faulting: The Mid-Atlantic Ridge, 15° 45′ N, *Geology* **30**, 879–882.

Melson, W.G., Hart, S.R., and Thompson, G., 1972, St. Paul's Rocks, Equatorial Atlantic: Petrogenesis, radiometric ages, and implications for sea-floor spreading, in R. Shagan (ed.), *Studies in Earth and Space Sciences: The Hess Volume*, pp. 241–272, Geological Society of America, Boulder, CO.

Miranda, E.A., John, B.E., Hirth, G. and Dick, H., 2002, Structural Development of an Oceanic Detachment Fault System, Atlantis Bank, Southwest Indian Ridge, *Eos Trans. AGU*, Fall Meeting.

Mutter, J.C. and Karson, J.A., 1992, Structural processes at slow-spreading ridges, *Science* **257**, 627–634.

Nooner, S.L., Sasagawa, G.S., Blackman, D.K. and Zumberge, M.A., 2003, Constraints on crustal structure at the Mid-Atlantic Ridge from seafloor gravity measurements made at the Atlantis Massif, *Geophys. Res. Lett.* **30**, 1446, doi:10.1029/2003GL017126.

O'Hanley, D.S., 1996, *Serpentinites. Records of Tectonic and Petrological History*, 277 pp., Oxford University Press, New York.

Parker, R., 1995, Improved Fourier terrain correction, part 1., *Geophys.* **60**, 1007–1017.

Pariso, J.E., Rommevaux, C. and Sempere, J.-C., 1996, Three-dimensional inversion of marine magnetic anomalies: Implications for crustal accretion along the Mid-Atlantic Ridge (28° – 31° 30'N), *Mar. Geoph. Res* **18**, 85–101.

Purdy, G.M., Sempéré, J.-C., Schouten, H., DuBois, D. and Goldsmith, R., 1991, Bathymetry of the Mid-Atlantic Ridge 24° –31° N: A map series, *Marine Geophysical Researches* **12**, 247–252.

Reston, T.J. Weinrebe, W., Grevemeyer, I., Flueh, E.R., Mitchell, N.C., Kirstein, L., Kopp, C. and Kopp, H., 2002, A rifted inside corner massif on the Mid-Atlantic Ridge at 5 degrees S, *Earth Planet. Sci. Lett.* **200**, 255–269.

Schroeder, T. and John, B.E., 2002, Microstructural evidence for low-temperature, brittle strain localization on an oceanic detachment fault: Atlantis Massif, 30° N, Mid-Atlantic Ridge, *Eos Trans. AGU*, Fall Meeting.

Schroeder, T., John, B.E. and Frost, B.R., 2002, Geologic implications of seawater circulation through peridotite exposed at slow-spreading mid-ocean ridges, *Geology* **30**, 367–370.

Schroeder, T., John, B.E., Kelley, D. and M.C. Participants, 2001, Microstructural observations of an 'oceanic core complex': Atlantis Massif, 30° N Mid-Atlantic Ridge, *Eos Trans. AGU* **82**, F1100.

Schroeder, T., 2003, Modes and implicatoins of mantle and lower crust denudation at slow-spreading mid ocean ridges, PhD thesis, University of Wyoming.

Searle, R.C., Patriat, P., Mével, C., Tamaki, F. and F.S. Team, 1998, TOBI side-scan imager and magnetics of the Southwest Indian Ridge III: Detailed history and tectonic style of sea-floor spreading and detachment faulting, *Eos Trans. AGU*, Fall Meeting.

Severinghaus, J.P. and Macdonald, K.C., 1988, High inside corners at ridge-transform intersections, *Mar. Geophys. Res.* **9**, 353–367.

Smith, D.K. and Cann, J.R., 1992, The role of seamount volcanism in crustal construction at the Mid-Atlantic Ridge (24° –30° N), *J Geophys. Res.* **97**, 1645–1658.

Treves, B. and Harper, G.D., 1994, Exposure of serpentinites on the ocean floor: Sequence of faulting and hydrofracturing in the northern Apennine ophicalcites, *Ofioliti* **19b**, 435–466.

Treves, B., Hickmott, D. and Vaggelli, G., 1995 Texture and microchemical data of oceanic hydrothermal calcite veins, Northern Appennine ophicalcites, *Ofioliti* **20**, 111–122.

Tucholke, B.E. and Lin, J., 1994, A geological model for the structure of ridge segments in slow spreading ocean crust, *J. Geophys. Res.* **99**, 11,931–11,958.

Tucholke, B.E., Juioka, K., Ishihara, T., Hirth, G. and Kinoshita, M., 2001, Submersible study of an oceanic megamullion in the central North Atlantic, *J. Geophys. Res.* **106**, 16,145–16,161.

Tucholke, B.E., Lin, J. and Kleinrock, M.C., 1998, Megamullions and mullion structure defining oceanic metamorphic core complexes on the Mid-Atlantic Ridge, *J. Geophys. Res.* **103**, 9857–9866.

Weissert, H.J. and Bernoulli, D., 1985, Transform margin in the Meoszoic Tehtys: evidence from the Swiss Alps. *Geol. Rundschau* **74**, 665–679.

Wernicke, B. and Axen, G.J., 1988, On the role of isostasy in the evolution of normal fault systems, *Geology* **16**, 848–851.

Zervas, C.E., Sempere, J.-C. and Lin, J., 1995, Morphology and crustal structure of a small transform fault along the Mid-Atlantic Ridge: The Atlantis Fracture Zone, *Marine Geophysical Researches* **17**, 275–300.